NASA TECHNICAL MEMORANDUM

NASA TM X-72803

NASA TM X-72803

MEASUREMENTS OF MEAN FLOW AND ACOUSTIC POWER FOR A SUBSONIC JET IMPINGING NORMAL TO A LARGE RIGID SURFACE

BY

Arthur P. Schloth
NASA/Grumman Industrial Research Associate

January 1976

NATIONAL AERONAUTICS AND SPACE ADMINISTRATION
LANGLEY RESEARCH CENTER, HAMPTON, VIRGINIA 23665

1. Report No.	2. Government Accession No.	3. Recipient's Catalog No.
NASA TM X-72803		

4. Title and Subtitle	5. Report Date
MEASUREMENTS OF MEAN FLOW AND ACOUSTIC POWER FOR A SUBSONIC JET IMPINGING NORMAL TO A LARGE RIGID SURFACE	January 1976
	6. Performing Organization Code
7. Author(s)	8. Performing Organization Report No.
Schloth, Arthur P.	
9. Performing Organization Name and Address	10. Work Unit No.
NASA-Langley Research Center Hampton, VA 23665	505-03-12
	11. Contract or Grant No.
	13. Type of Report and Period Covered
12. Sponsoring Agency Name and Address	NASA Technical Memorandum
National Aeronautics and Space Administration Washington, DC 20546	14. Sponsoring Agency Code

15. Supplementary Notes

The research was performed while the author was a Grumman Industrial Research Associate. The author is currently employed by Aeroflex Laboratories, Inc.

16 Abstract

An experimental study was made to measure the mean flow field and acoustic power of a subsonic jet impinging normal to a large rigid surface. A 6.25 cm diameter, circular cool air jet was used at heights of 20, 10, and 5 jet diameters above the surface. The jet exit Mach number was varied from 0.28 to 0.93. Impact and static pressure surveys were made in directions both axial and lateral to the jet axis and also parallel and perpendicular to the surface. Acoustic power was calculated from microphone measurements made during each test run using a diffuse field calibration for the test facility. Results indicate that the flow field for jet impingement is characterized mainly by a strong rise in static pressure in the impingement region near the surface and by boundary layer development in the wall jet region. Acoustic power measurements generally followed a U^8 law for both the free jet and jet impingement although there was some variation especially at high Mach number and for close impingement distances. Overall noise levels increased with decreasing jet-to-surface height. Normalized power spectra correlated well for all cases when the Strouhal number was greater than 0.2; the correlation was poor when the Strouhal number was low.

17 Key Words (Suggested by Author(s))	18. Distribution Statement
Jet impingement, flow-surface noise impingement noise	Unclassified Unlimited

19. Security Classif. (of this report)	20. Security Classif. (of this page)	21 No. of Pages	22. Price*
Unclassified	Unclassified	48	$3.75

*For sale by the National Technical Information Service, Springfield, Virginia 22161

Measurements of Mean Flow and Acoustic Power For A Subsonic Jet Impinging Normal to a Large Rigid Surface

by

Arthur P. Schloth

SUMMARY

An experimental study was made to measure the mean flow field and acoustic power of a subsonic jet impinging normal to a large rigid surface. A 6.25 cm diameter, circular cool air jet was used at heights of 20, 10, and 5 jet diameters above the surface. The jet exit Mach number was varied from 0.28 to 0.93. Impact and static pressure surveys were made in directions both axial and lateral to the jet axis and also parallel and perpendicular to the surface. Acoustic power was calculated from microphone measurements made during each test run using a diffuse field calibration for the test facility. Results indicate that the flow field for jet impingement is characterized mainly by a strong rise in static pressure in the impingement region near the surface and by boundary layer development in the wall jet region. Acoustic power measurements generally followed a U^8 law for both the free jet and jet impingement although there was some variation especially at high Mach number and for close impingement distances. Overall noise levels increased with decreasing jet-to-surface height. Normalized power spectra correlated well for all cases when the Strouhal number was greater than 0.2; the correlation was poor when the Strouhal number was low.

INTRODUCTION

With the current applications of impinging jet flows for STOL aircraft and air cushion vehicles, and with concurrent requirements for low noise aircraft, this research was conducted to investigate some related characteristics of the mean flow field and acoustic radiation of a normal impinging jet. Numerous studies have been made of the flow field of impinging jets. Among the more recent comprehensive studies in which the mean and turbulent characteristics of impinging jets were measured are the experimental surveys conducted by Donaldson and Snedeker (ref. 1), Hrycok, Lee and Gauntner (ref. 2), and Brady and Ludwig (ref. 3). Investigations have also been made of the acoustic radiation of impinging jets. However, in most cases they have included additional noise effects due to flow at the edge of the surface or over a flexible surface. Some studies of this nature have been conducted by Olsen, Miles and Dorsch (ref. 4) and Hayden (ref. 5).

The purpose of this experiment was to study both the fluid dynamics and the acoustics of a circular subsonic jet impinging on a large rigid surface. Results are presented on the mean flow field and acoustic power for a jet impinging perpendicular to the surface.

The experimental tests were conducted in the NASA Langley 55 foot Vacuum Cylinder where subsonic jet flow at the exit (6.25 cm diameter circular nozzle) of the test apparatus was produced by the pressure difference of internal partial vacuum and external atmospheric pressure. The experimental configurations were that of a free jet and impinging jet at various heights (20, 10, and 5 jet diameters) above the surface. For each configuration, tests at several Mach numbers from .28 to .93 were conducted. Due

to the favorable reverberant room characteristics of the test facility, suitable experimental conditions were present to measure the acoustic diffuse field. Acoustic power was calculated for all test cases. Also, by automated and remotely controlled experimental equipment, mean flow surveys of the flow field both in the jet and near the surface were conducted. Results of the experimental measurements are presented as mean velocity profiles, static pressure distributions, total acoustic power levels and acoustic power spectra in third octave bands.

SYMBOLS

α	Local fluid speed of sound, m/s
B	Chamber barometric pressure, inches of Mercury (mm of Mercury)
D	Inner diameter of the jet, m
f	Frequency, Hz
f_c	Third octave band center frequency, Hz
L	Impingement height of jet exit to surface, m
$\bar{L}_p$	Average third octave band sound pressure level, dB ref. .00002 N/m^2
L_w	Third octave band sound power level, dB ref. 10^{-12} watts
M_{ex}	Jet exit Mach number
P_a	Measured differential static pressure relative to ambient chamber pressure, N/m^2
P_c	Measured chamber internal ambient pressure, N/m^2
P_L	Measured absolute static pressure, N/m^2

P_o	External (atmospheric) pressure, N/m^2
P_s	Measured differential impact pressure relative to ambient chamber pressure, N/m^2
P_t	Measured absolute impact pressure, N/m^2
P_i	Mean sound pressure microphone measurement, N/m^2
P_o	Sound pressure reference level, .00002 N/m^2
R	Radial coordinate along plate from the center of impingement, m
T_c	Measured chamber internal ambient temperature, ^oR
$\bar{T}_{60}$	Average reverberation time, s
U	Vertical velocity component of flow, m/s
U_{ax}	Jet axial vertical velocity, m/s
U_{ex}	Jet exit velocity for free jet cases, m/s
$\bar{U}_{ex}$	Jet exit velocity for impingement cases, m/s
V	Radial velocity component of flow, m/s
V_o	Volume of test chamber, ft^3 (m^3)
V_s	Surface radial velocity, m/s
Z	Vertical coordinate above plate, m
Z'	Axial distance from jet exit, m
ρ	Local fluid mass density, kg/m^3
μ	Local fluid viscosity, $N-s/m^2$
$\dot{m}$	Jet exit mass flow rate, kg/s

TEST SYSTEM DESCRIPTION

Test Apparatus

The test apparatus (fig. 1) was designed so that a subsonic turbulent jet could exhaust at selected heights above a large flat rigid surface. The NASA Langley 55 foot vacuum cylinder (fig. 2) with an internal air volume of 3794 cubic meters was used as a blow down facility to induce a subsonic jet flow at the exit of the test apparatus. By controlling the cylinder low pressure conditions, a uniform jet flow was obtained at the exit of a circular cross section of pipe, 6.25 cm in diameter. A bellmouth inlet port external to the cylinder induced smooth uniform flow at low velocity through a 6 meter long, 24 cm diameter flexible rubber hose inside the vacuum cylinder. The 24 cm hose was attached to a fixture which allowed the exit of the pipe jet to be positioned at selected heights above the impinged surface. The flow cross section was contracted at the fixture to induce high velocity flow through the 4 meters of 6.2 cm inner diameter pipe. A curved section was made in the pipe to orient the pipe jet exit normal to the plate. A straight section of 1.5 meters after curvature and a final .5 meter section of smooth machined aluminum pipe yielded a uniform velocity profile at the pipe exit.

Internal cylinder conditions were monitored to within 1 mm Hg accuracy by a Hasting pressure gauge. A pneumatically controlled conical inlet port plug was used to regulate the jet flow. Operating times were controlled to minimize errors due to pressure equalization in the vacuum cylinder to 3 mm of Hg/minute at low internal pressures.

The rigid impinged surface was made of aluminum alloy 2.9 meters by 1.8 meters and 2.54 cm thick. It was fastened about its perimeter to a 5 inch

steel channel. Rubber material was used between the plate and the channel to damp vibrations. The point of jet impingement was at least .9 meter from any edge of the plate.

Test Procedure

The experiments were conducted with the pipe jet directed downward at various heights. The test conditions included the free jet and impingement cases of 20, 10, and 5 jet-diameters above the surface, with jet exit Mach numbers ranging from .28 to .93. Some preliminary tests were conducted to check the stability of the test apparatus, jet exit flow conditions, background noise, and reverberant room characteristics.

The jet exit flow conditions were first calibrated by an impact pressure probe measurement across the jet exit. The chamber operating conditions were then used to produce the desired jet exit velocities. The stability of the test apparatus was monitored by accelerometer measurements on the pipe jet during operating conditions. The test facility was also evaluated for suitable reverberant room characteristics. The criteria for using the facility as a reverberant room was that there were adequate volume, shape, and wall absorption to diffuse the sound field so that the acoustic spectra was nearly uniform throughout the room. A diffuse field calibration procedure was conducted to evaluate the reverberant room characteristics using three microphone locations. The calibration procedures are described in Appendix A.

Due to the axisymmetry of a normal impinging jet, only a two dimensional survey of the flow field was necessary. The jet axial velocity decays were determined from impact and static pressure measurements using the formulation of Appendix B. The decay of radial velocity of the jet flow spreading over the

surface was calculated from the measured total head pressure of an impact probe resting on the surface. Boundary layer total pressure profiles were measured at several radial stations from the stagnation point for the cases of impingement. However, both impact pressure and static pressure measurements were determined to be inaccurate in the impingement region due to high turbulence and large lateral velocity components due to the deflected flow. Therefore, impact and static pressure measurements were made only at heights greater than one jet diameter above the surface and impact pressure measurements of the boundary layer profiles were made only at radial stations at least one jet diameter from the center of impingement.

The impact pressure was measured by a probe of .05 cm outer diameter hypodermic tubing, and static pressure measured using the static ports on a round nose .16 cm outer diameter Pitot probe. The sensitivity of the pressure transducer instrumentation yielded resolution to .01 mm of mercury. D.C. volt digital output of the pressure profiles were recorded on magnetic tape with a digital data acquisition system. The lateral pressure profiles were measured by traversing the impact and static probe in tandum on a mechanism that allowed slow uniform lateral motion. The jet axial pressure profiles as well as boundary layer profiles along the plate were measured with an impact probe while traversing vertically either along the jet centerline or at a radial station.

The acoustic measurements were made during a set of runs independent than those for the flow measurements. For all test conditions (i.e. Free jet, L/D = 20, 10, 5) the acoustic pressure data were taken with three 12.7 mm. condenser microphones at separate positions in the chamber. The measured noise was recorded on a multi channel tape recorder and the sound pressure

level spectra were analyzed later using a 1/3 octave band real time analyzer. The arithmetic average of the sound pressure levels from the three microphone positions was used along with the calibrated average reverberation times of the chamber to calculate the acoustic power spectrum.

During each of these tests accelerometer measurements were also made to determine the surface accelerations due to the jet flow impingement. These accelerations were found to be negligible in all runs.

DISCUSSION OF RESULTS

Mean Flow Results

Using the terminology defined in references 2 and 7, the mean flow characteristics of jet impingement can be separated into four characteristic regions.

Referring to figure 3, the first region is called the jet mixing region. It extends from the nozzle exit to the end of the potential core. The uniform velocity core interacts with the ambient air forming a highly turbulent surrounding mixing region. This mixing region dissipates the uniform mean velocity of the potential core.

The second region is designated the transition region. It starts immediately at the end of the potential core and is characteristic of axisymmetric free turbulent jet flow. The axial decay of velocity and spreading becomes proportional to the downstream axial distance.

The third region is designated the impingement region and is characterized by unsteady turbulent flow and deflected flow patterns essentially induced by the back pressure from the point of impingement. The impingement region is

therefore marked by an axial velocity deceleration and a regime of increased static pressure.

The fourth region is called the wall jet region. It begins where the radial surface velocity starts to decay due to spreading, and the surface boundary layer thickness increases. The transition from the impingement region is rapid and the wall jet region forms established radial flow with self-similar mean velocity profiles.

The mean flow results for the free jet and the three impingement cases, L/D = 20, 10, and 5, are presented in Figures 4-8. All the mean velocity data have been non-dimensionalized by the free jet case exit velocity, U_{ex}. Static pressure has been non-dimensionalized by the vacuum cylinder internal pressure. The data are presented for jet exit velocities of 293., 186., and 98. m/sec.

From figure 4-a to 4-c the jet axial static pressure in the impingement region is seen to be positive relative to ambient. This is typical of the impingement case where a back pressure at the surface causes an upstream effect of more positive static pressure and therefore reduced upstream velocities. The results of the axial velocity surveys are also presented in figures 4-a to 4-c. The axial extent of the constant velocity potential core is shown to vary only slightly with the exit velocity and impingement height (except, of course, for the L/D = 5 case, where the core never fully dissapates before the effect of the plate is felt). The effects of increased static pressure due to flow stagnation in the impingement region are shown to extend 1 or 2 jet diameters above the impinged surface.

A radial decay of the total head pressure slightly above the surface was measured to determine the extent of the impingement region and the flow spreading over the surface. The radial velocity decays, as presented in

figures 5-a to 5-c, were calculated by assuming local static pressure equal to ambient. The impingement region is nominally defined to extend radially from the stagnation point (R/D = 0) to the position where the radial surface velocity begins to decrease (between 0.4 and 1.8 jet diameters). This decrease in radial velocity near the surface designates a transition point to radial spreading of the impingement region. As expected, the impingement region is largest for the largest L/D case.

The boundary layer profiles of the jet spreading over the plate were also surveyed and results for the 293 m/sec velocity case are presented in figures 6-a to 6-c. The boundary layer surveys were made at radial distances of one to five jet diameters from the stagnation point. The velocity profiles illustrate the extent of the surface shear layer. A nominal boundary layer thickness δ, defined as the position of local peak velocity and shown by the dashed curve on the figures, separates this shear layer from the turbulent mixing region of the wall jet. From the boundary layer profiles the radial flow can be seen to diffuse rapidly due to radial spreading over the surface. At outer radial positions from about 3 to 5 jet exit diameters the boundary layer profiles approach a similar shape independent of the jet-to-plate separation distance. This wall jet profile is characterized by reduced shear stress at the wall and a fully developed turbulent velocity profile.

Surveys of the lateral mean velocity profiles and lateral static pressure distributions were made for the free jet case of 293 m/sec and are presented in figure 7. The alterations of the mean flow structure for the cases of impingement are given in figures 8 and 9, at one and two diameter heights above the impinged surface. The velocity profiles at 1 and 2 diameters above

the impinged surface are shown not to differ much from the profiles of the corresponding free jet locations at $Z'/D = 4, 8, 19$. However the measured static pressure distributions to indicate a change due to back pressure effects for the impingement cases. It must be noted that the static pressure measured near the impinged surface may include turbulent dynamic pressure and therefore may be in error. Therefore only qualitative results are indicated by these lateral velocity profiles and static pressure distributions.

Acoustic Results

The acoustic radiation from a normal impinging jet is due to jet noise and impingement noise sources. Jet noise is modelled classically as convected quadrupole patterns, and a dimensional analysis of the dependence of the sound field can be given in terms of a typical velocity U in the flow, a characteristic length ℓ, and the density ρ and speed of sound α of the external atmosphere (ref. 8). The analysis shows that for nonconvected quadrupole like radiation from turbulent flow, the total sound power P is proportional to

$$\frac{\rho \ell^2 U^8}{\alpha^5}$$

The jet noise components of free jets are included in the acoustic power measurements on impinging jets. For the cases of normal jet impingement the characteristic free jet regions have been deflected and spread uniformly over the large rigid surface. The designated impingement and wall jet regions may present additional effects as noise producing regions. Since the impinged

surface is large and rigid, the acoustic radiation measured will include the reflection of the local acoustic quadrupole sources of the flow (ref. 9). The magnitude of quadrupole source reflections depends on the location and scale of the sources near the surface.

For a large rigid surface, there is no dipole sound radiation due to the flexibility of the surface or from flow discontinuities at the edges of the plate. However, a dipole source term can exist due to the fluctuating viscous shear stress at the bounding solid surface (ref. 10). The additional acoustic power radiated from such a dipole source term may be taken to be proportional to the sixth power of the velocity near the surface.

The diffuse field sound pressure level measurements were made for each impingement case at the same chamber pressure ratios as listed for the free jet cases in Table II. Three microphone measurements were made and the average sound pressure levels in the third octave bands were calculated. The acoustic power spectra and total acoustic power were calculated following the procedures for diffuse field noise measurements outlined in Appendix A.

The total acoustic power levels are presented in figure 10. For each jet exit velocity, the data show the free jet and 20-jet-height power levels to be within $\pm$1dB of each other. As the jet-height is lowered to 10 and 5, the power level increases. The results correlate to the 'U^8' law for all conditions with the exception of the highest velocity, L/D = 5 case. However, as will be shown later in this report, a unique feedback phenomena was present which resulted in increased power levels at this condition. These results indicate that the quadrupole source terms predominate for jet impingement and the source terms become larger as the jet height is lowered.

Third octave power spectra are presented in figures 11-a to 11-d for each run. The data shows the broadband nature of the noise and similar shaped distributions independent of the velocity. The 2000 hertz tone apparent in the L/D = 5 data is believed to be caused by an acoustic standing wave. The flow measurements show that for the 293 m/sec free jet, the jet potential core extends approximately 5 jet diameters and therefore the basic fluid structure exists for an acoustic standing wave from flow-surface interactions. This tonal radiation for close cases of impingement and high jet exit Mach number has been studied in greater depth in reference 11.

Power spectral data normalized to the overall power levels are plotted against the dimensionless jet exit Strouhal number ($f_c\ D/\bar{U}_{ex}$) in figures 12-a to 12-h. The peak Strouhal number is seen to be generally concentrated in the .2 to .3 band for most cases. For the high velocity, L/D = 5 cases, the peak is slightly higher. Spectral shapes agree very well for the high Strouhal numbers; the agreement becomes poor at the lower Strouhal numbers.

The power spectral data calculated from the third octave band levels were also normalized to the respective free jet overall acoustic power level ($OAPWL_{f_j}$) and plotted in figures 13-a to 13-c. These plots make more evident the deviation of the acoustic power spectral density and spectra frequency content of the impingement cases from the respective free jet case. For the cases of impingement the spectra frequency content becomes more concentrated the closer the case of impingement. Therefore additional sources of acoustic radiation have contributed noise in addition to the broadband free jet mixing noise.

CONCLUSIONS

An experimental study has determined mean flow parameters and acoustic power radiation for numerous cases of a normally impinging 6.2 cm-diameter cold air jet. From static and total head pressure probe surveys, mean velocity profiles and static pressure distributions were calculated. The mean flow measurements were used to define the various flow regions of impinging jets. For subsonic flow at jet impingement heights of 20, 10, and 5 jet diameters, the impingement region was noted to extend from the stagnation point to 1 to 2 jet diameters upstream and from .4 to 1.8 jet diameters radially. The radial decay of velocity spreading over the impinged surface and the boundary layer mean velocity profiles showed the flow to be independent of jet height by the time the flow was three nozzle diameters away from the jet axis.

The acoustic sound pressure levels were measured in a reverberant field and the acoustic power spectra and overall acoustic power calculated by diffuse field procedures. Acoustic power measurements generally followed a U^8 law for both the free jet and jet impingement, although there was some variation especially at high Mach number and for close impingement distances. Normalized power spectra correlated well for all cases when the Strouhal number was greater than 0.2; the correlation was poor when the Strouhal number was low.

APPENDIX A

Reverberant Field Measurement Procedures

The procedures for calculating acoustic sound power spectrum from measured sound pressure levels in a reverberant field were used as specified in the ASA Standard S 1.2. The following procedures specified in reference 12 were used to determine the suitability of the test chamber as a reverberant room.

(1) An evaluation of the diffuse field characteristics was made by three microphone measurements in the test chamber. The microphone locations complied with the requirements that they be at least a 1/4 wavelength from the room surfaces for the lowest frequency of interest.

(2) A broad band "white noise" source was positioned where the impinging jet would be typically located above the rigid plate during testing. The source and the impinged surface were located in the test chamber complying with the requirements that they be at least 1/4 wavelength away from all surfaces of the room.

(3) A diffuse field calibration was made by instantaneous switch - offs of the "white noise" source and measurement of the mean-square pressure level decay with time at each microphone in each filtered third octave band of interest. These calibration tests were conducted at ambient pressure conditions in the chamber equal to atmospheric.

(4) Incorporating the diffuse field calibration, the sound power spectrum of an impinging jet source in the test chamber can be calculated by the following equation from S1.2 subsection 3.5.10.

APPENDIX A

$$L_w = \overline{L}_p + 10 \log_{10} V_0 - 10 \log_{10} \overline{T}_{60} - 29.5 + C_2 \qquad \text{(A 1)}$$

where:

L_w - the sound power level in decibels referenced to 10^{-12} watt for all frequency bands of interest.

$\overline{L}_p$ - the average sound pressure level, of the three microphone measurements, in decibels referenced to 0.0002 microbar.

V_0 - the total air volume of the reverberation chamber in cubic feet.

$\overline{T}_{60}$ - the average reverberation time, determined from the diffuse field calibration, for the frequency bands considered with the source in place.

C_2 - $10 \log_{10} (30/B)$, a correction to standard atmosphere

B - baromatric pressure in inches of mercury

Using equation (A1), the acoustic power spectra was calculated for the average sound pressure level measured in the reverberation room. A background noise correction is included in the final values used for $\overline{L}_p$ in the calculations. To not only illustrate the results of equation (A1) but to validate the diffuse field measurements, sample measurements are presented in figures 14 and 15. Experimentally acceptable agreement is shown by three microphone measurements in the Reverberant room during a test. These results along with the indicated background noise of figure 14 were used to calculate the L_p and L_w spectrum of figure 15.

APPENDIX B

Flow Field Calculation Procedures

The desired flow results were calculated from the measured quantities using the equations given in reference 13. Using the notation

P_s - Stagnation pressure (differential pressure)

P_a - Static pressure (differential pressure)

P_c - Ambient chamber pressure (absolute pressure)

T_c - Ambient chamber temperature (degrees Rankine)

T_t - Stagnation temperature (degrees Rankine),

the local Mach number for steady isentropic flow is given by

$$M_L = \sqrt{\frac{2}{k-1}\left[\left(\frac{P_L}{P_t}\right)^{\frac{1-k}{k}} - 1\right]} \tag{B-1}$$

where

$$P_t = P_s + P_c \tag{B-2}$$

is the total (stagnation) pressure, and

$$P_L = P_a + P_c \tag{B-3}$$

is the local (static) pressure. The local velocity (U_L) is then calculated from the measured dynamic pressure by the Bernoulli Equation for compressible flow:

APPENDIX B

$$(P_t - P_L) = 1/2\ \rho_L\ U_L^2\ (1 + M_L^2/\ 4 + (2-k)\ M_L^4/\ 24 + ..) \qquad (B-4)$$

where ρ_L is the local density. Assuming that the jet total temperature is equal to the external chamber temperature T_t, the local temperature is given by

$$T_L = T_t \left(\frac{P_L}{P_t} \right)^{\frac{k-1}{k}} \qquad (B-5)$$

and therefore

$$\rho_L = P_L / RT_L \qquad (B-6)$$

The jet exit Reynolds number was calculated from

$$R_n = \rho_L\ U_L\ D\ /\ \mu \qquad (B-7)$$

where μ is the local fluid viscosity given by Sutherland's formula

$$\mu = 108.7\ \frac{T_L^{1.5}}{T_L - 198.6}\ X\ 10^{-8} \qquad (B-8)$$

and the jet exit mass flow rate was obtained from:

$$\dot{m} = \int^{A_j} \rho_L\ U_L\ dA \qquad (B-9)$$

where A_j is the jet exit cross sectional area.

REFERENCES

1. Donaldson, C. D.; and Snedeker, D. S.: A Study of Free Jet Impingement. Part 1, Mean Properties of Free and Impinging Jets. J. Fluid Mechanics, vol. 45, pp. 281-319, 1971.

2. Hrycok, P.; Lee, D. T.; Gauntner, J. W.; and Livingood, J. N. B.: Experimental Flow Characteristics of a Single Turbulent Jet Impinging on a Flat Plate. NASA TN D-5690, March 1970.

3. Brady, W. G.; and Ludwig, G.: Theoretical and Experimental Studies of Impinging Uniform Jets. Cornell Aeronautical Lab Report BB-1657-S-1, 1963.

4. Olsen, W. A.; Miles, J. H.; and Dorsch, F. G.: Noise Generated by Impingement of a Jet Upon a Large Flat Board. NASA TN D-7075, Dec. 1972.

5. Hayden, R. E.: Noise from Interaction of Flow with Rigid Surfaces, A Review of Current Status of Prediction Techniques, NASA CR 2126, Oct. 1972.

6. Donaldson, C. D.; Snedeker, R. S.; and Margolis, D. P.: A Study of Free Jet Impingement. Part 2, Free Jet Turbulent Structure and Impingement Heat Transfer. J. Fluid Mech., vol. 45, pp. 477-512, 1971.

7. Gauntner, J. W.; and Livingood, J. N. B.: Survey of Literature on Flow Characteristics of a Single Turbulent Jet Impinging on a Flat Plate. NASA TN D-5652, Feb. 1970.

8. Lighthill, M. J.: On Sound Generated Aerodynamically II. Turbulence as a Source of Sound. Proc. Roy. Soc. (London), A222, pp. 1-32, 1954.

9. Powell, A.: Aerodynamic Noise and the Plane Boundary. Journal of the Acoustical Society of America, vol. 32, no. 8, Aug. 1960.

10. Fuchs, H. V.; and Michalke, A.: Introduction to Aerodynamic Noise Theory, Progress in Aerospace Sciences, vol. 14, pp. 227-297, 1973.

11. Wagner, F. R.: The Sound and Flow Field of a Axially Symmetric Free Jet Upon Impact on a Wall. NASA TT F-131942, Oct. 1971.

12. American Standards Association: American Standard Method for the Physical Measurement of Sound. Section S1.2, Aug. 1962.

13. Ames Research Staff: Equations, Tables, and Charts for Compressible Flow. NACA Report 1135, 1953.

TABLE I MEASURED FLOW PARAMETERS

Chamber Pressure Ratio (Pc/Po)	Impingement Distance (L/D)	Jet Exit Velocity (Uex, m/s)
.46	5	286.4
.52	5	261.3
.59	5	233.6
.66	5	204.2
.72	5	179.9
.79	5	153.6
.86	5	123.4
.92	5	92.1
.46	10	290.4
.52	10	267.5
.59	10	239.7
.66	10	212.7
.72	10	185.5
.79	10	161.1
.86	10	129.6
.92	10	91.4
.46	20	290.6
.52	20	268.5
.59	20	242.7
.66	20	214.7
.72	20	186.2
.79	20	158.8
.86	20	132.4
.92	20	97.9

TABLE II FREE JET EXIT FLOW CONDITIONS.

Chamber Pressure Ratio (Pc/Po)	Jet Exit Mach No. (M_{ex})	Jet Exit Velocity (U_{ex}) m/s	Jet Exit Reynolds Number	Mass Flow Rate ($\dot{m}$) kg/sec
.46	.93	293.0	7.40×10^5	.585
.52	.83	266.0	7.27×10^5	.576
.59	.74	238.0	7.00×10^5	.566
.66	.64	212.0	6.62×10^5	.546
.72	.55	186.0	6.16×10^5	.516
.79	.47	159.0	5.59×10^5	.474
.86	.38	130.0	4.82×10^5	.424
.92	.28	98.0	3.83×10^5	.332

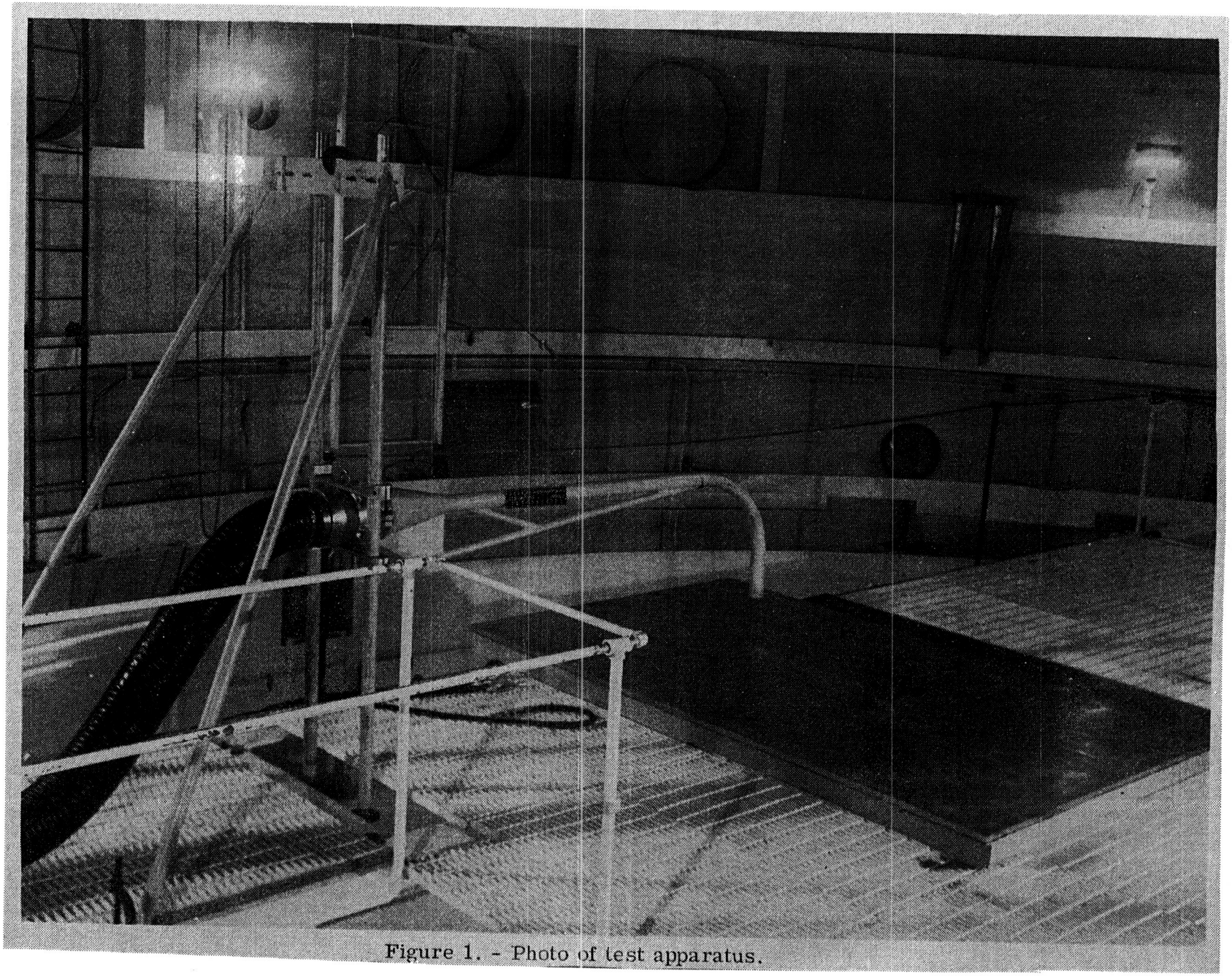

Figure 1. - Photo of test apparatus.

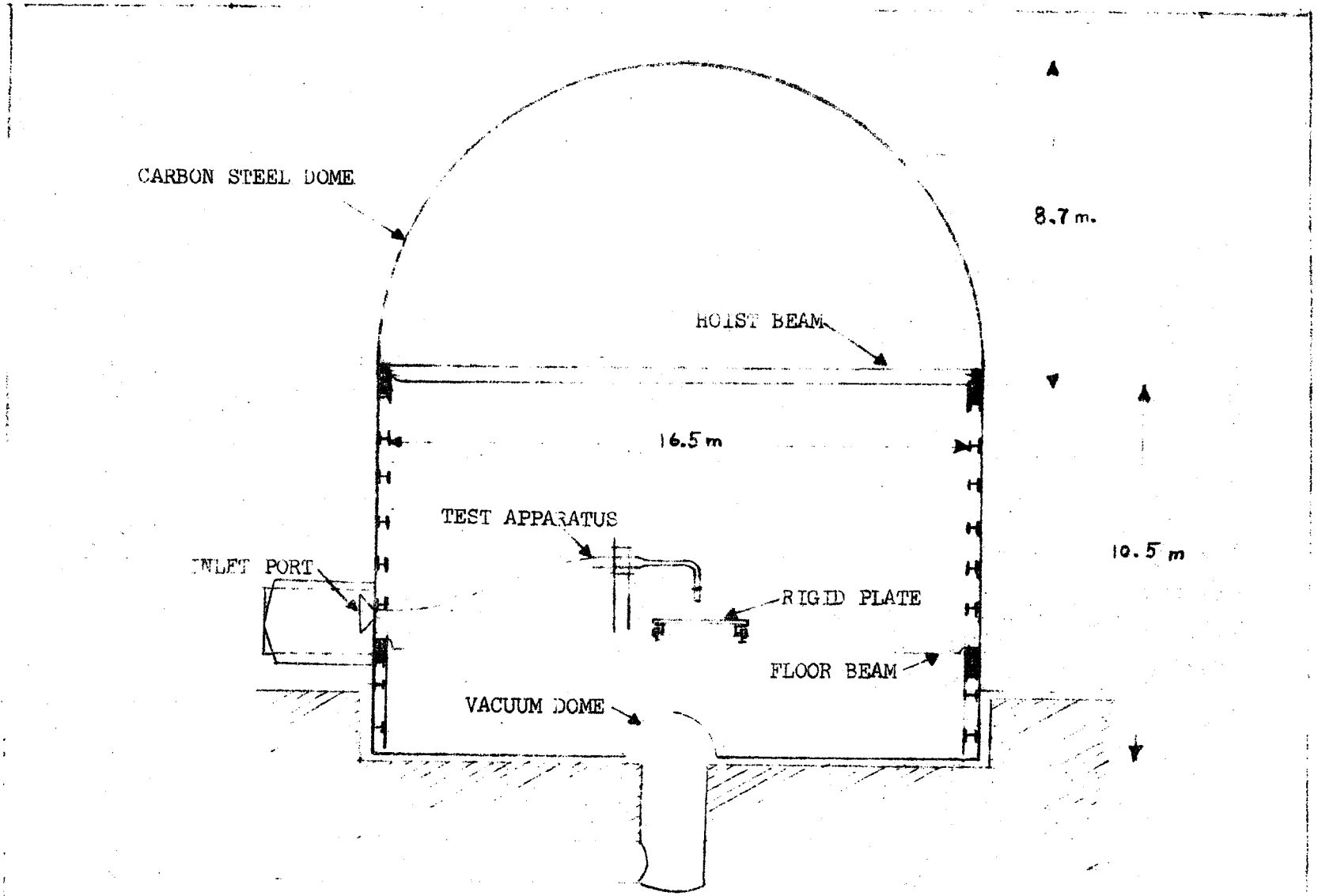

Figure 2. - Sketch of test facility.

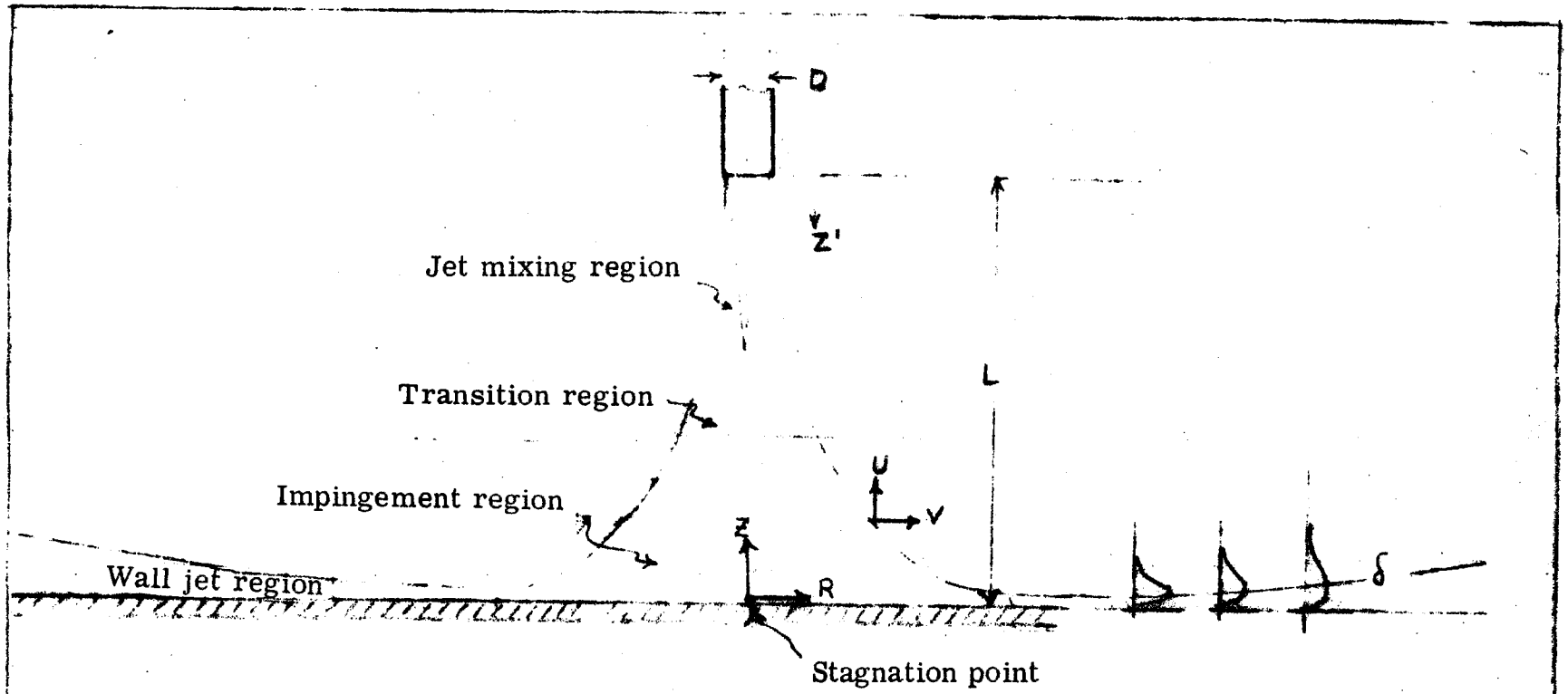

Figure 3. - Mean-flow characteristic regions of impinging jet and coordinate-system definition.

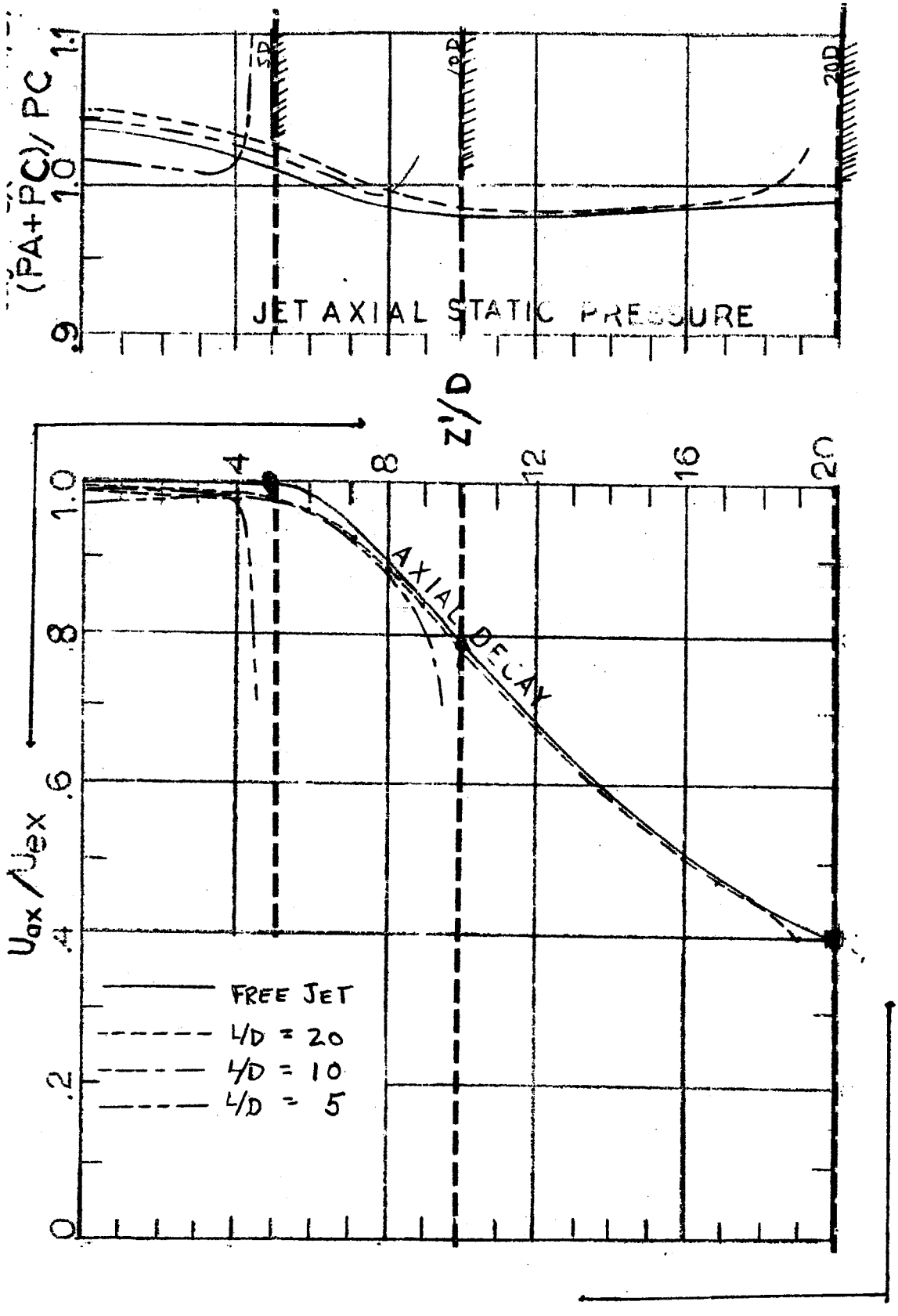

(a) U_{ex} = 293 m/s

Figure 4. - Axial distributions of velocity and static pressure.

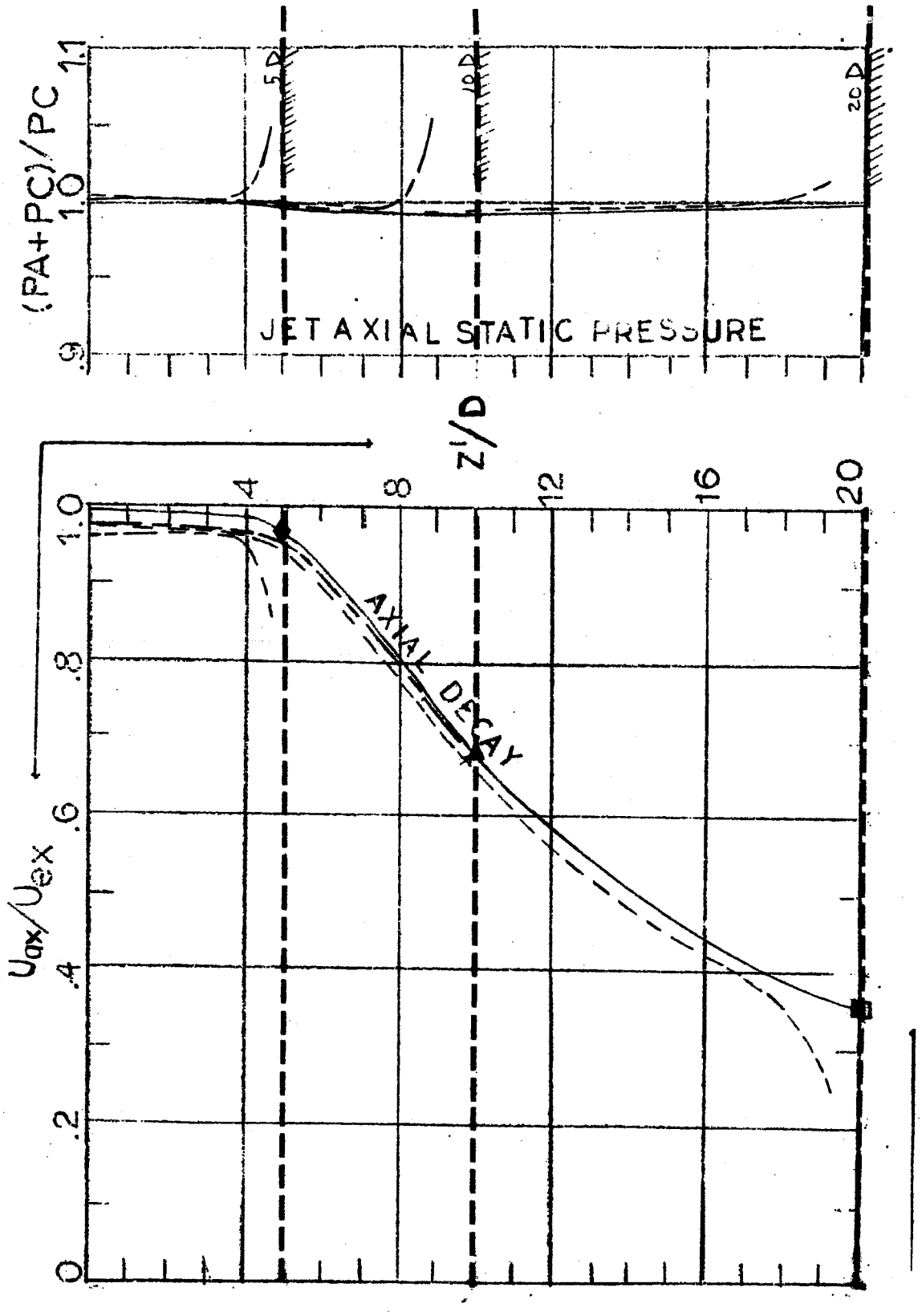

(b) U_{ex} = 186 m/s

Figure 4. - Continued

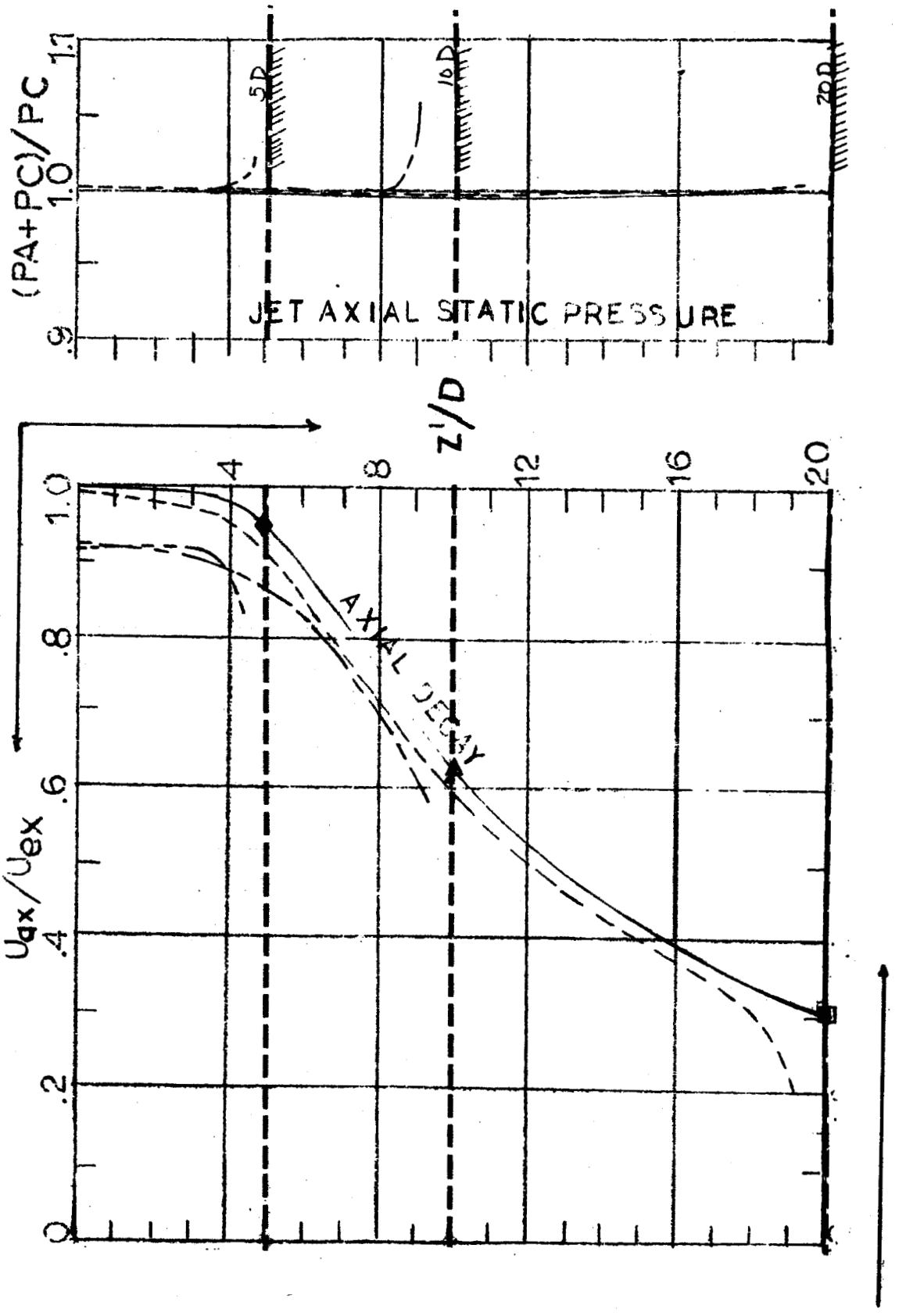

(c) U_{ex} = 98 m/s

Figure 4. - Concluded.

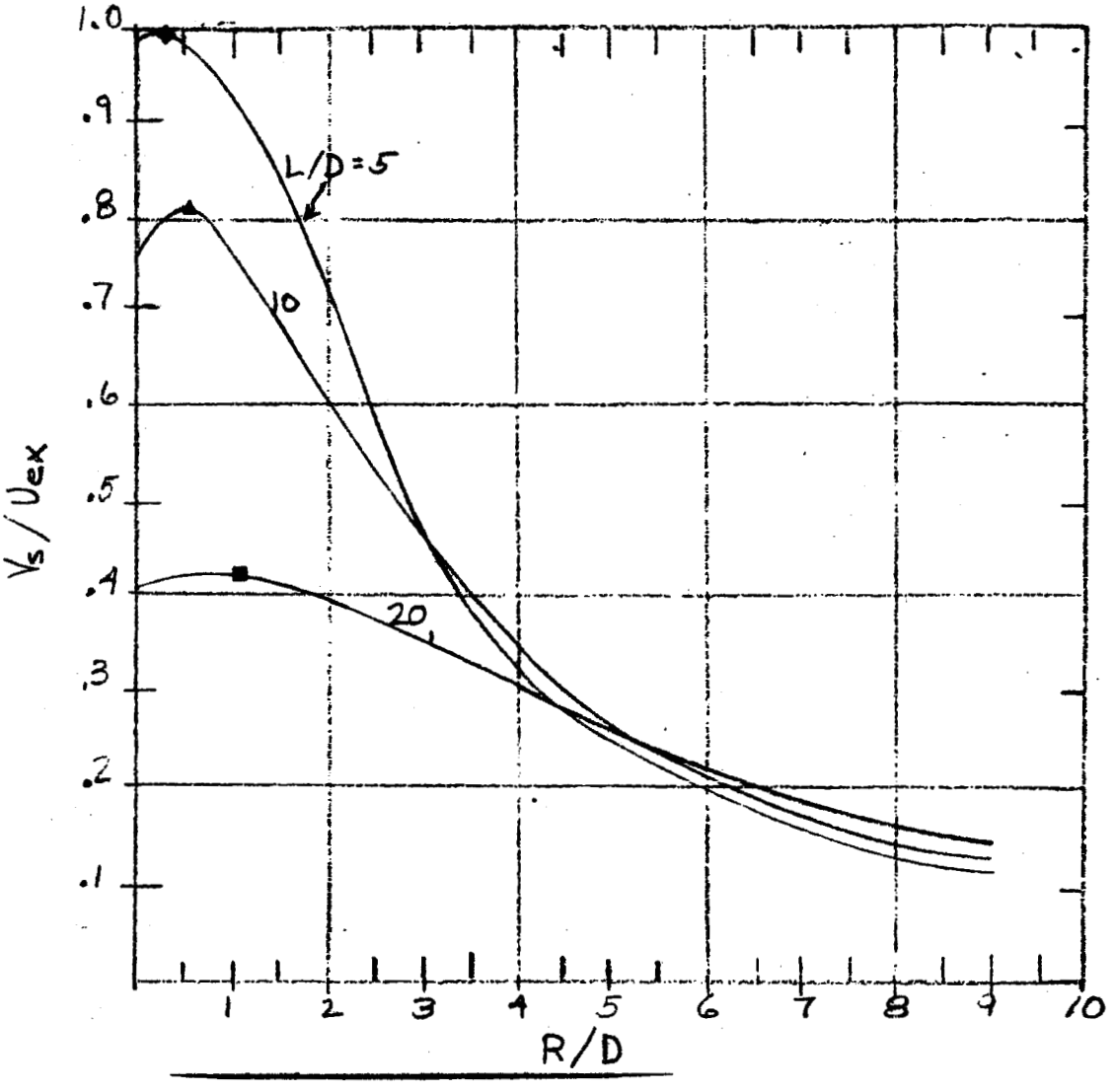

(a) U_{ex} = 293 m/s

Figure 5. - Radial distribution of velocity near surface.

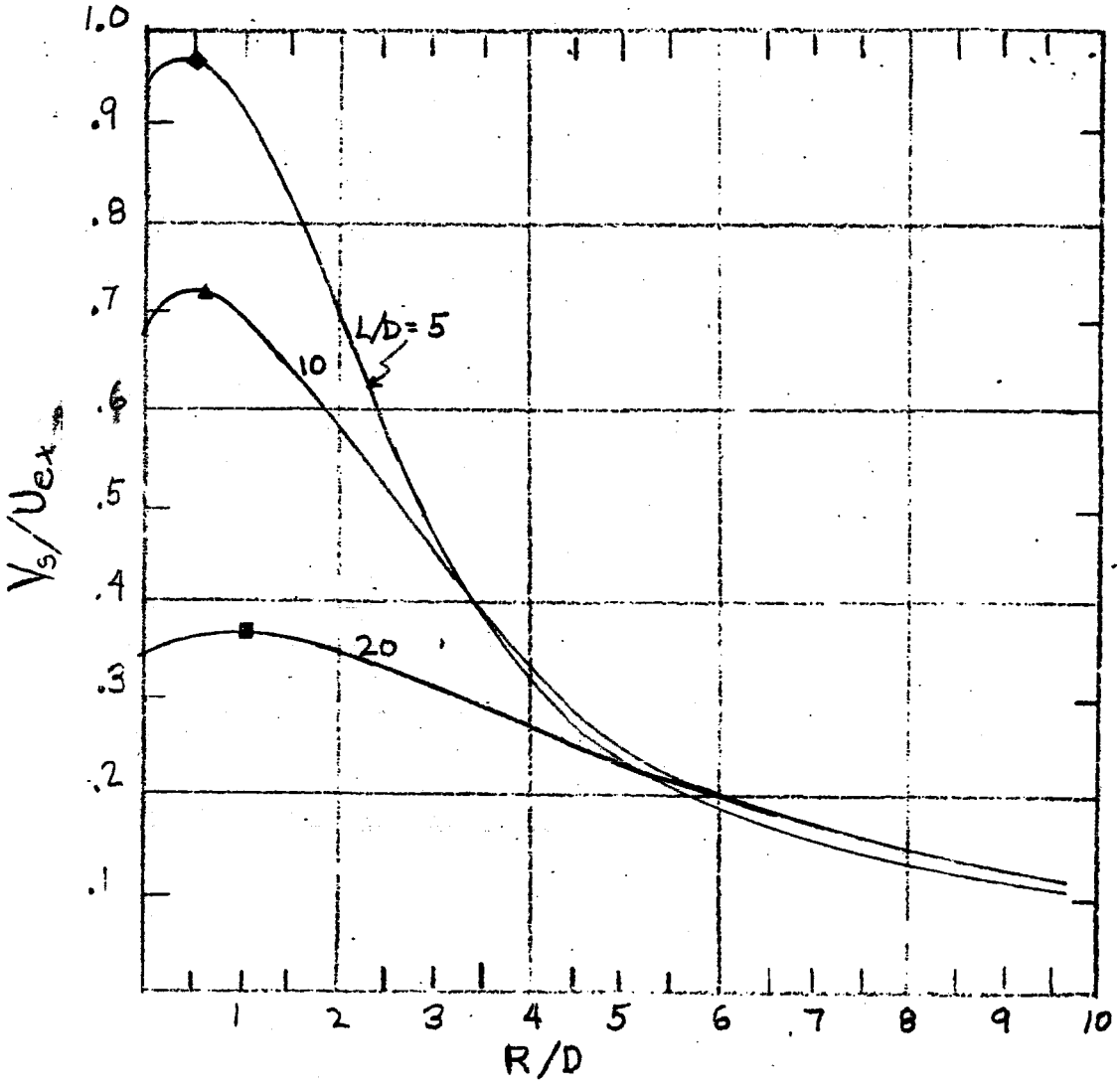

(b) U_{ex} = 168 m/s

Figure 5. - Continued.

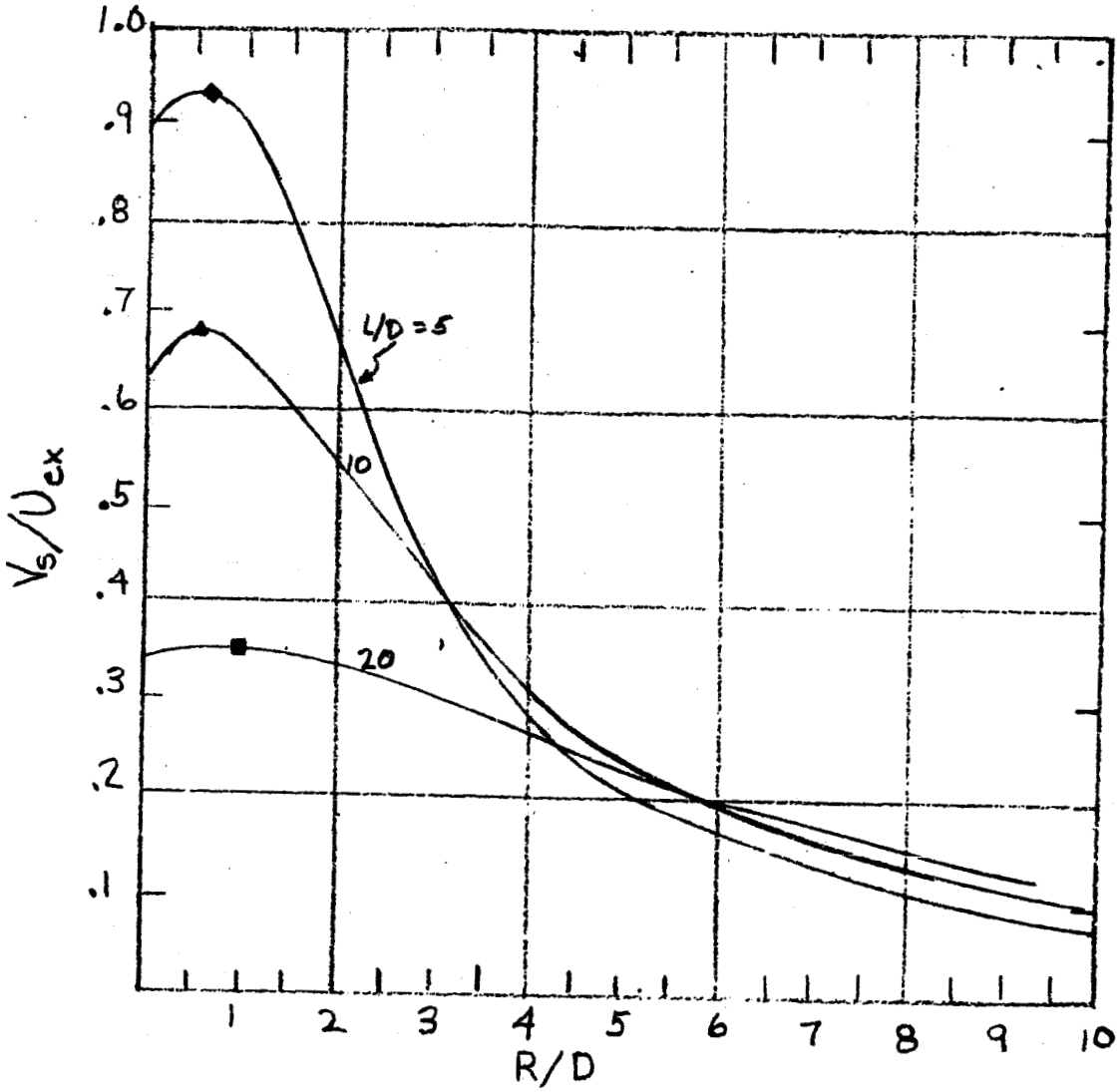

(c) U_{ex} = 98 m/s

Figure 5. - Concluded

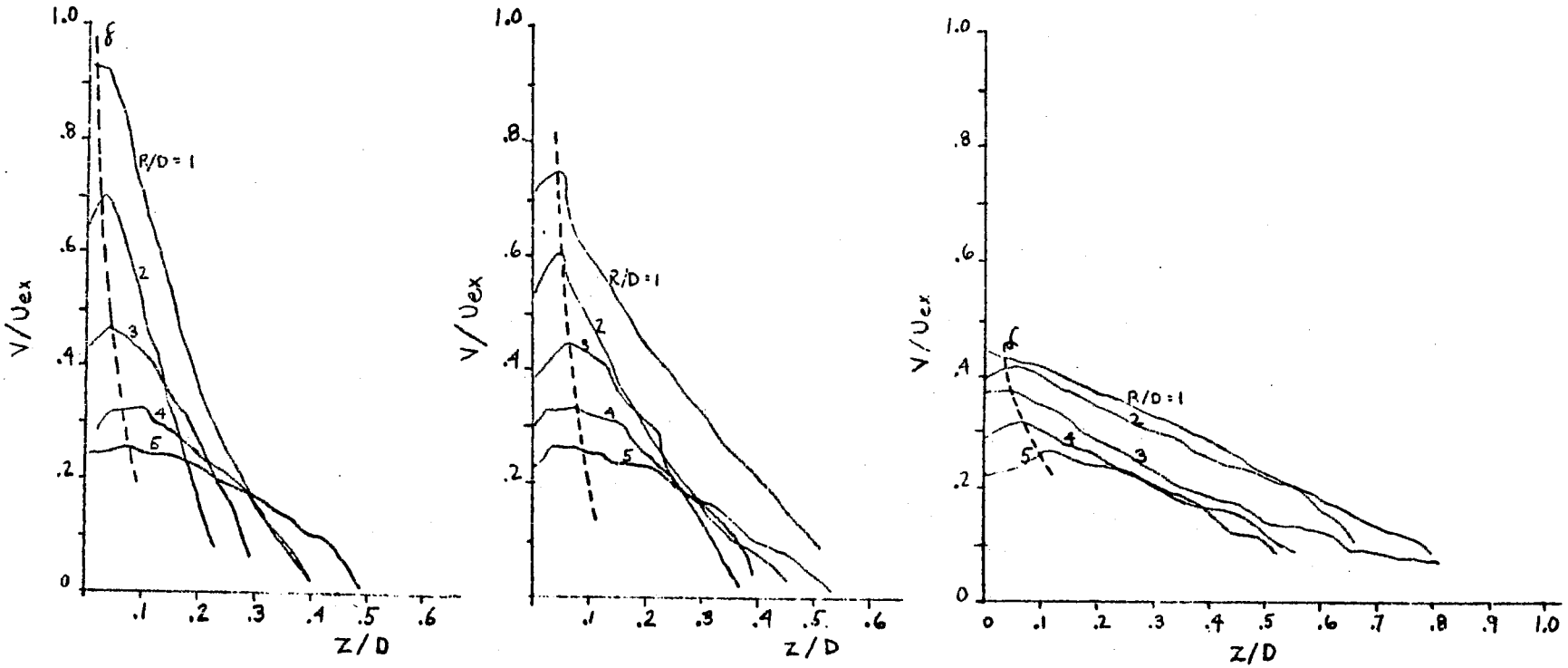

(a) L/D = 5 (b) L/D = 10 (c) L/D = 20

Figure 6. - Boundary layer profiles at various radial distances from stognation point. U_{ex} = 293 m/s.

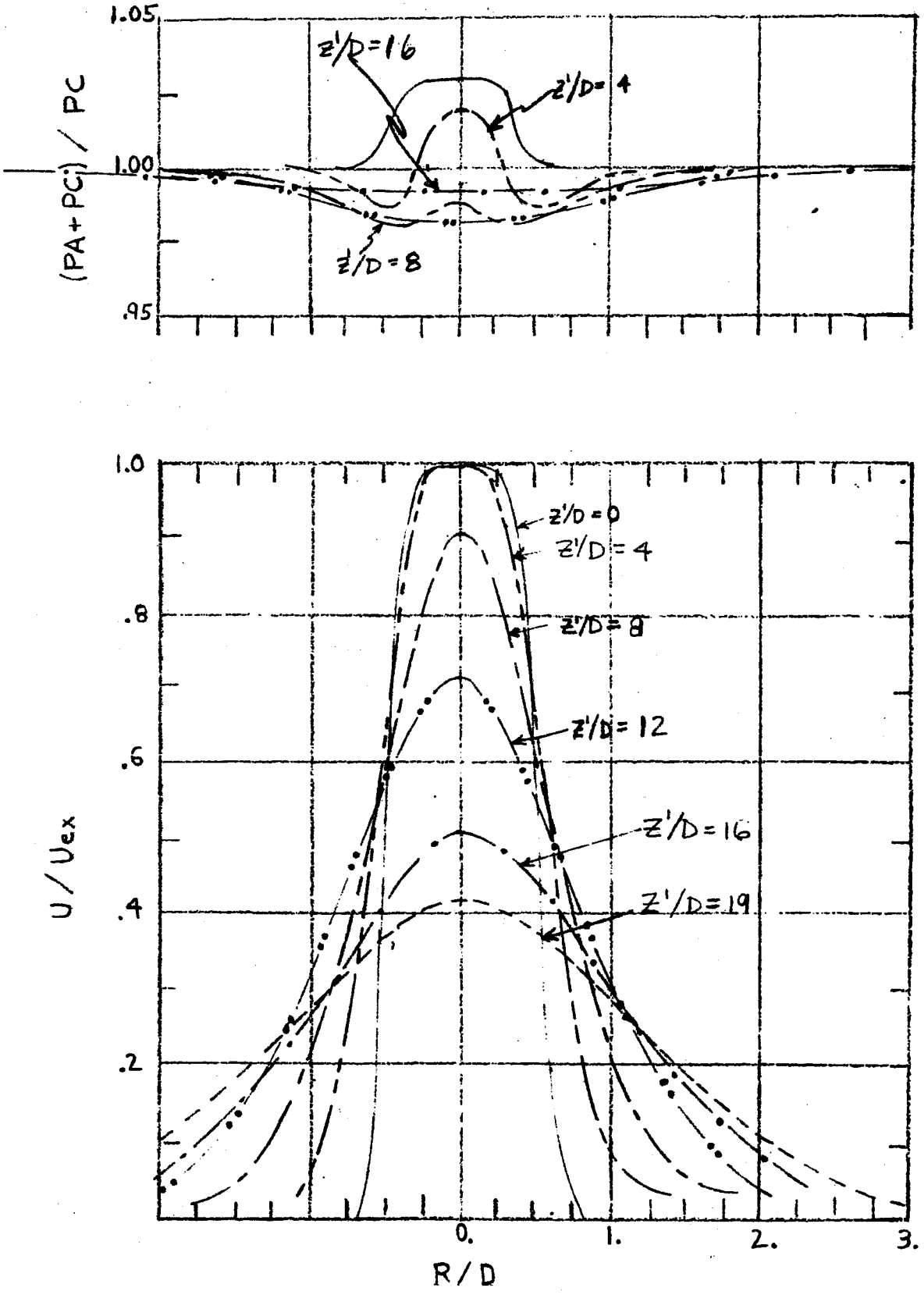

Figure 7. - Radial distributions of velocity and static pressure at various distances from jet exit. Free jet case. U_{ex} = 293 m/s.

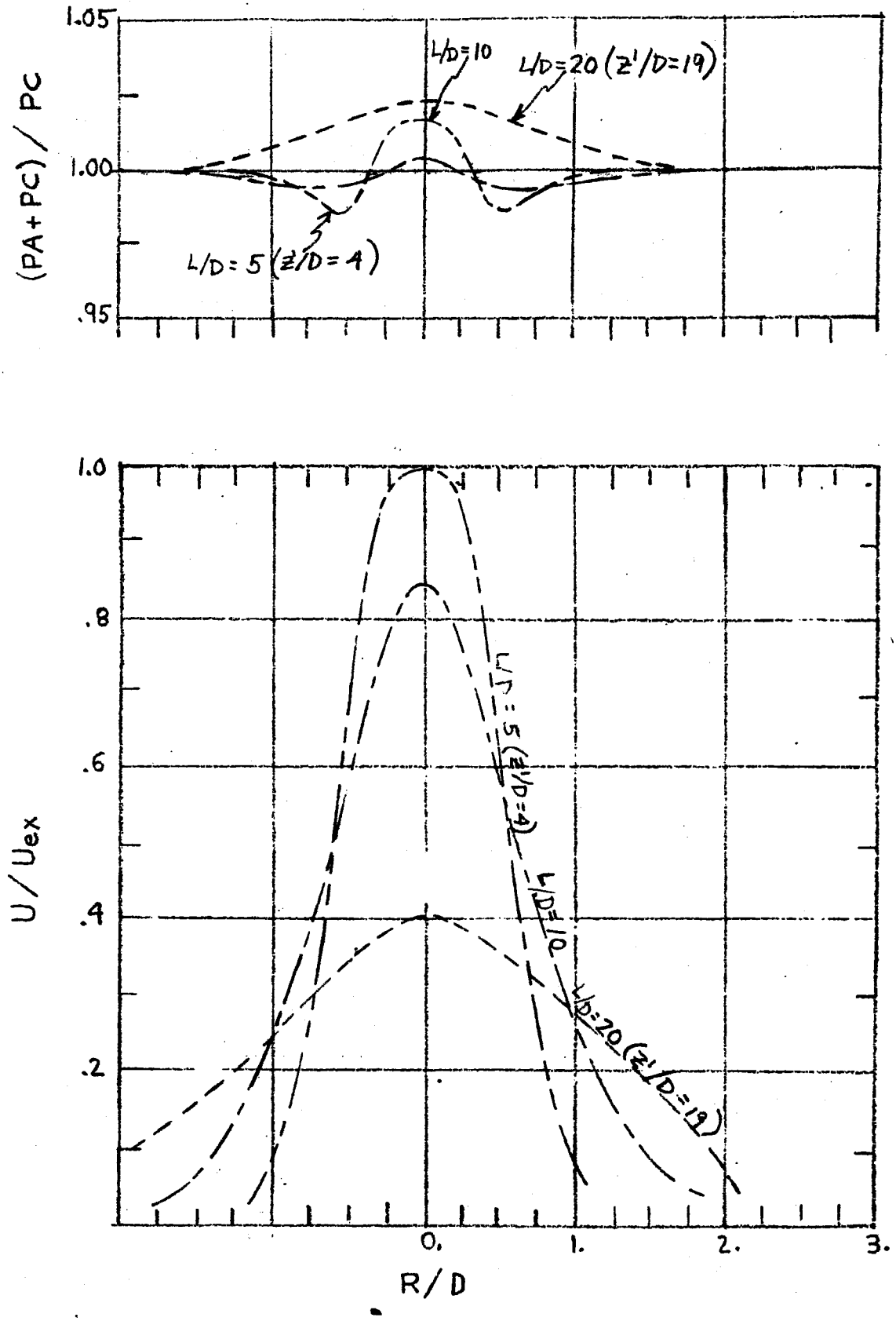

Figure 8. - Radial distributions of velocity and static pressure at z/D = 1. Impingement cases. U_{ex} = 293 m/s.

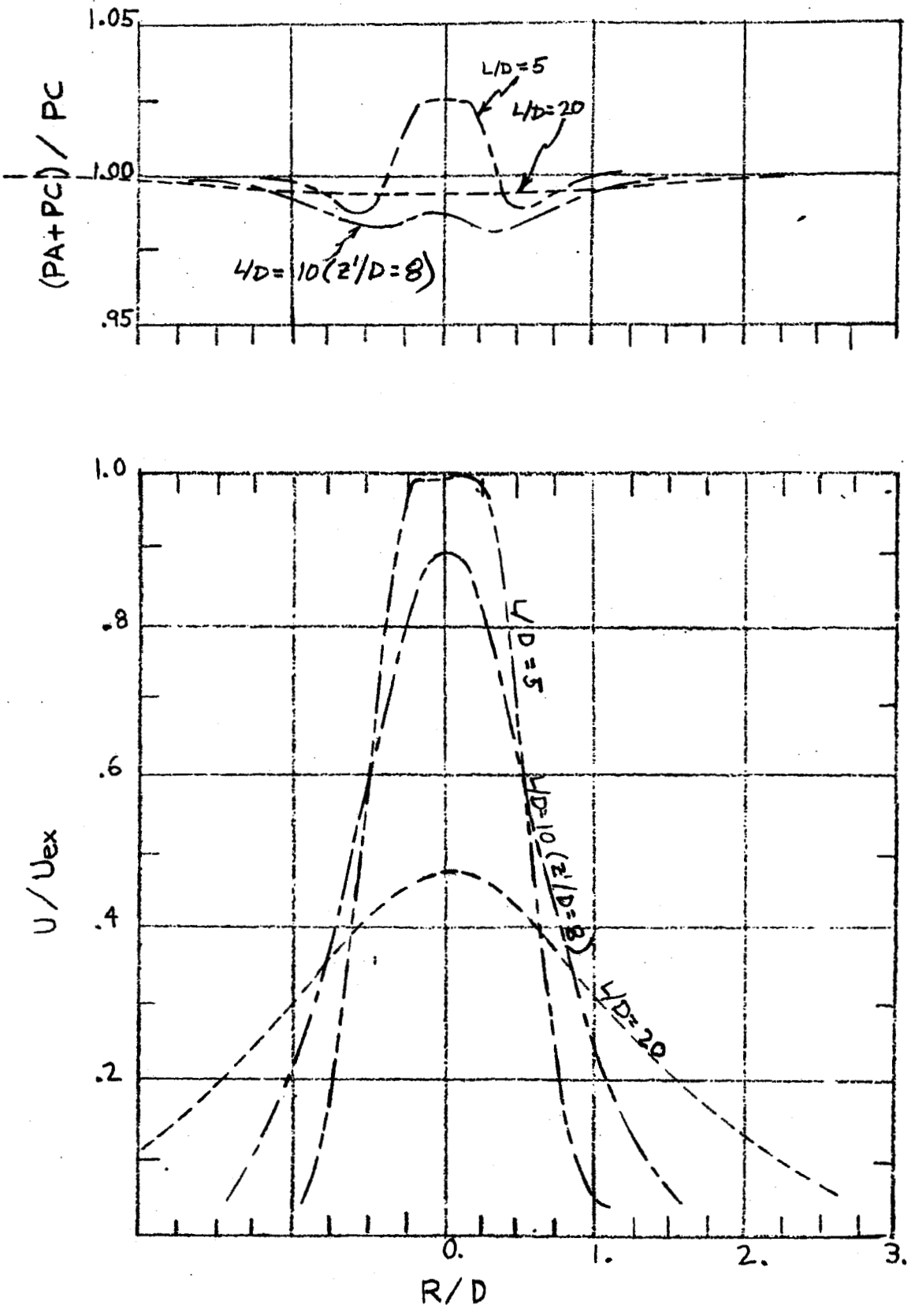

Figure 9. - Radial distributions of velocity and static pressure at z/D= 2.

Impingement cases. U_{ex} = 293 m/s.

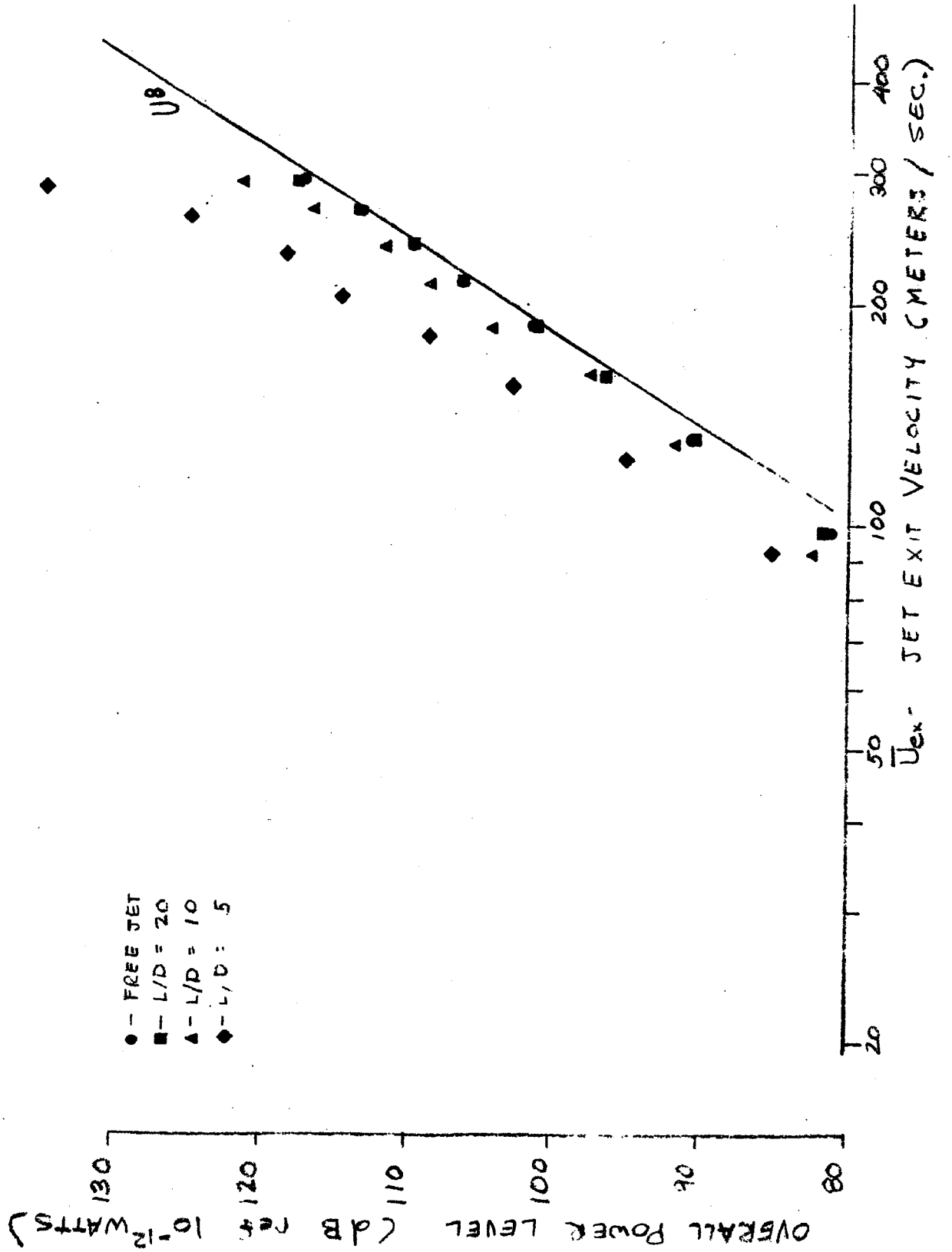

Figure 10. - Total acoustic power versus jet exit velocity.

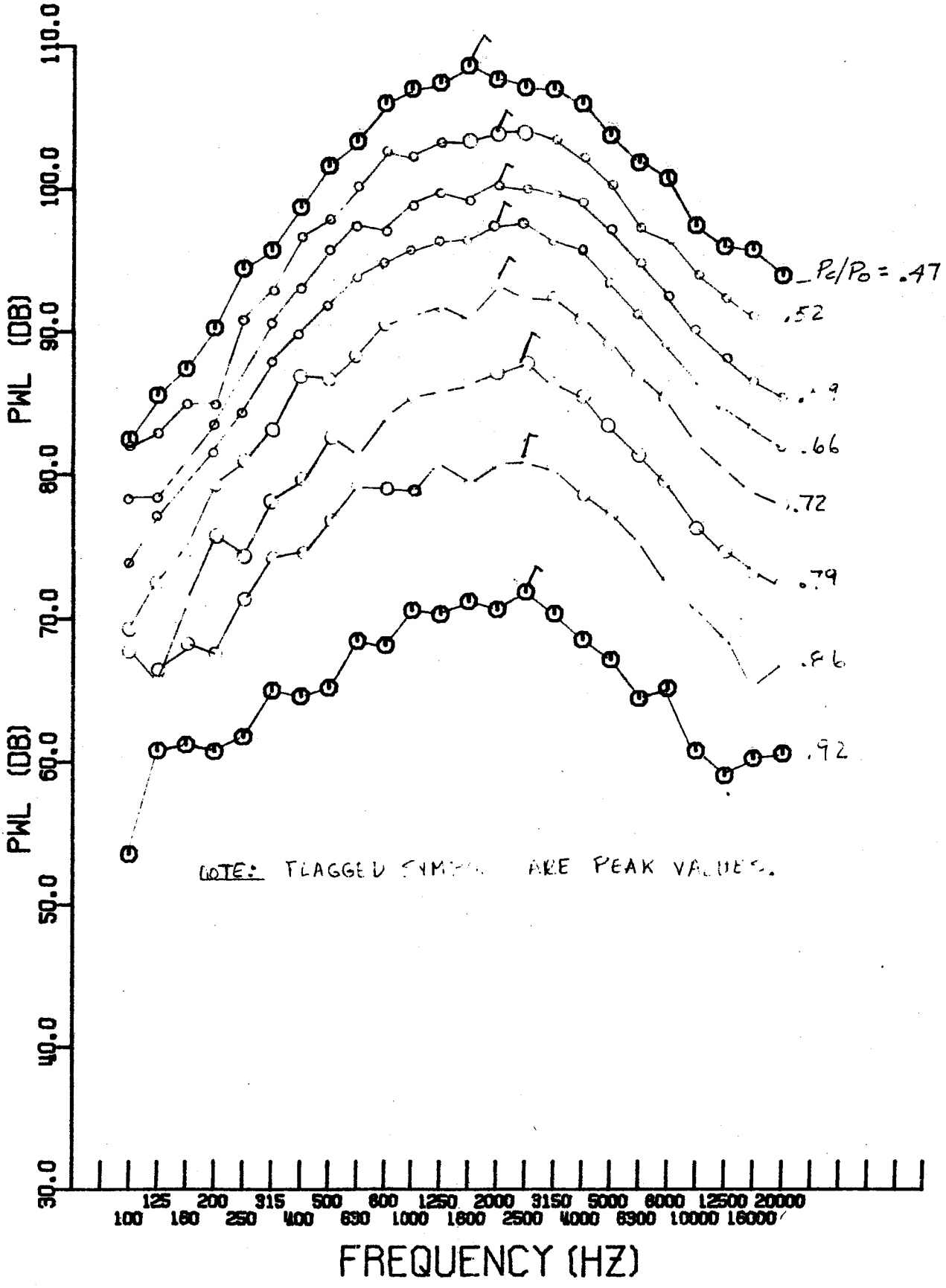

(a) Free jet

Figure 11. - One-third octave power spectra.

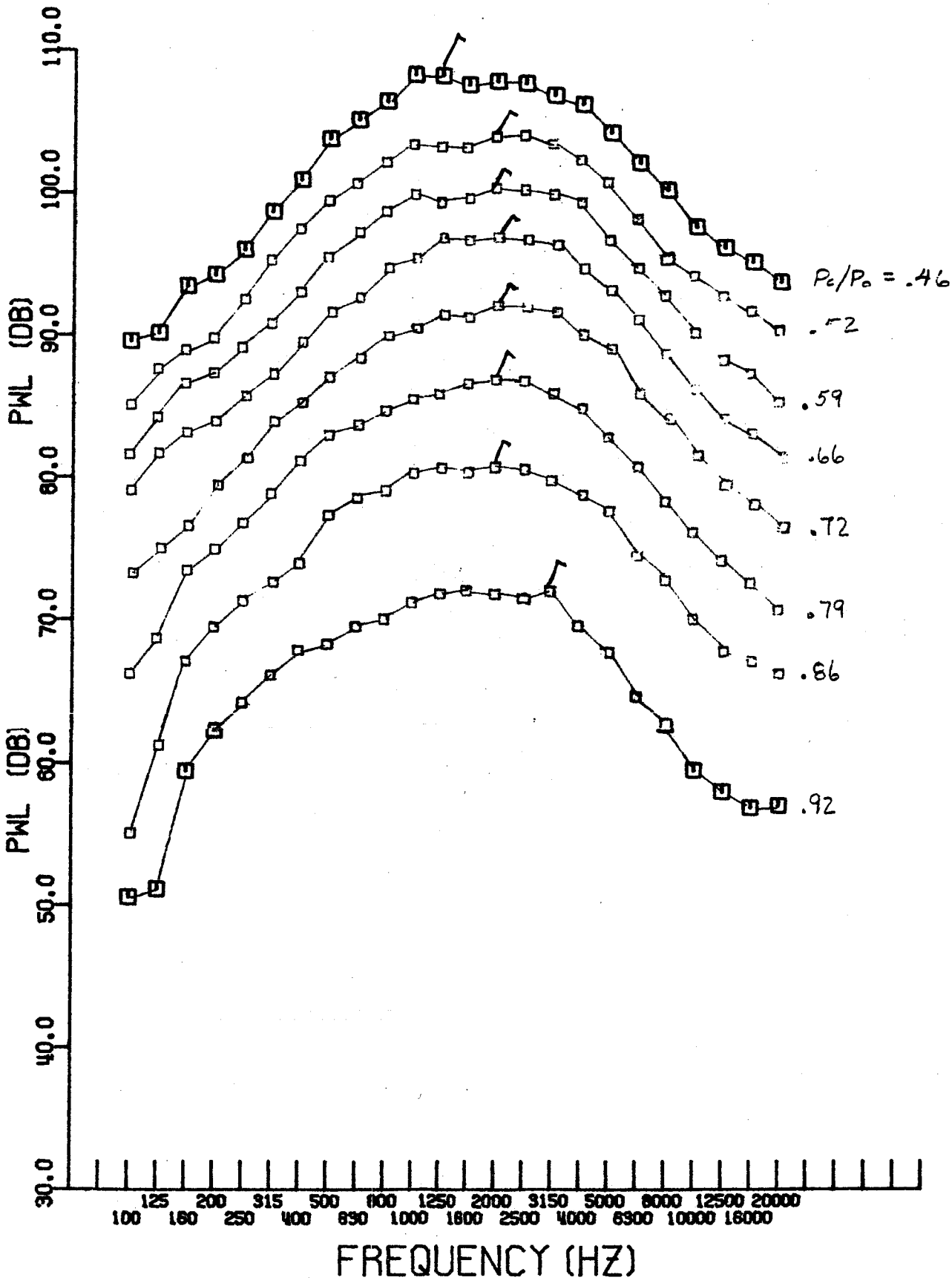

(b) L/D = 20

Figure 11. - Continued.

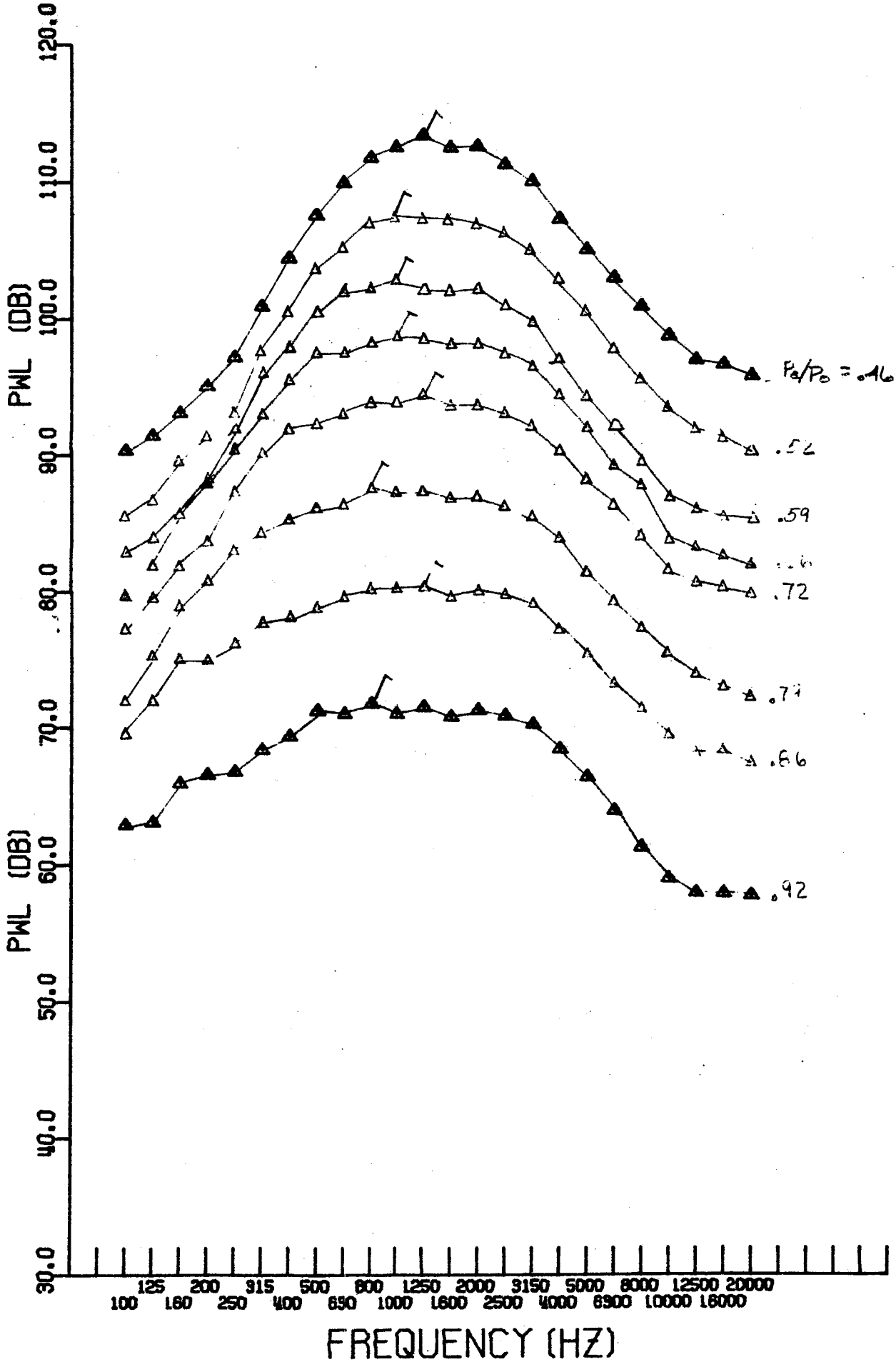

(c) L/D = 10

Figure 11. - Continued.

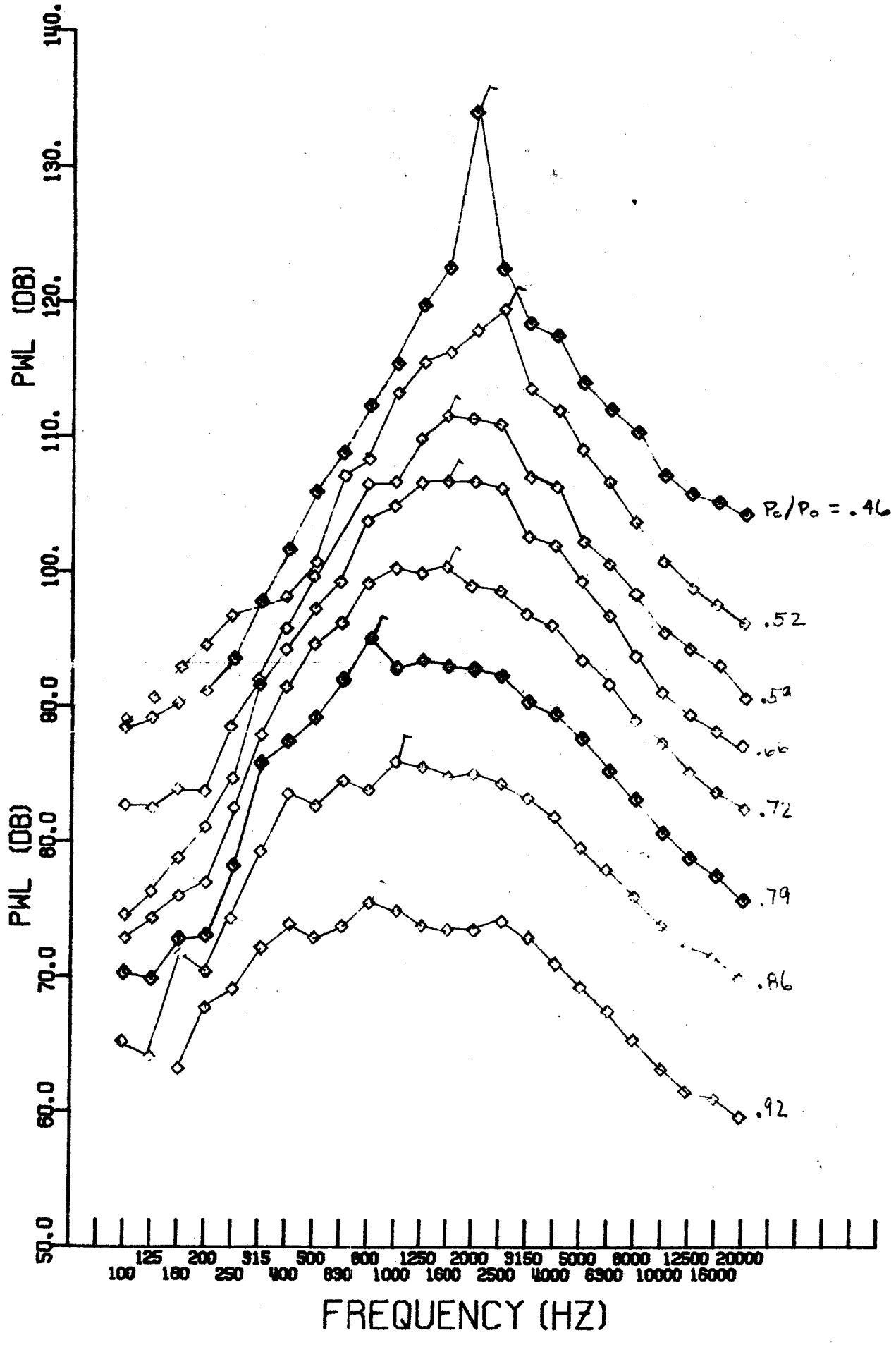

(d) L/D = 5

Figure 11. - Concluded.

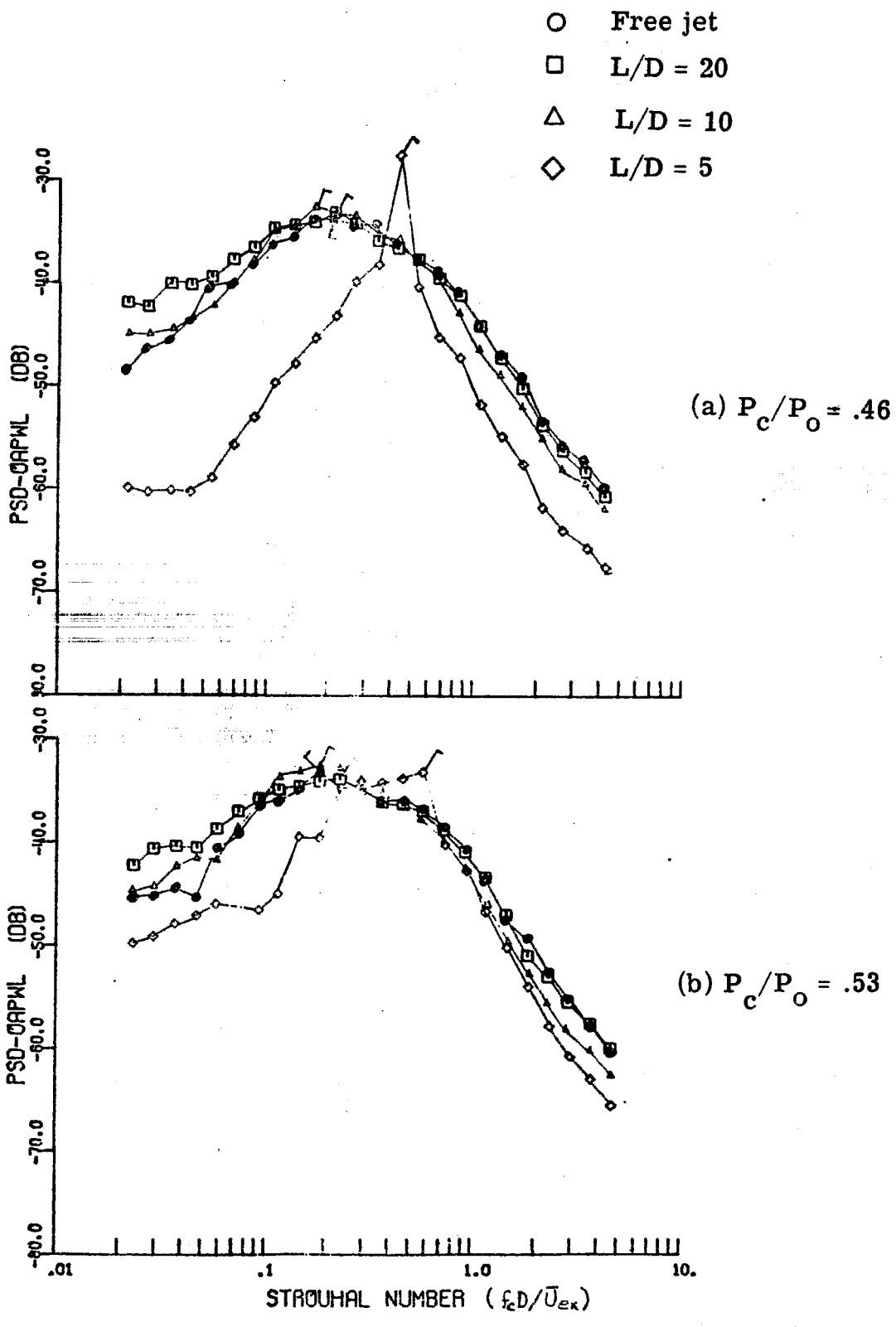

Figure 12. - Power spectra normalized to overall power levels for jet impingement.

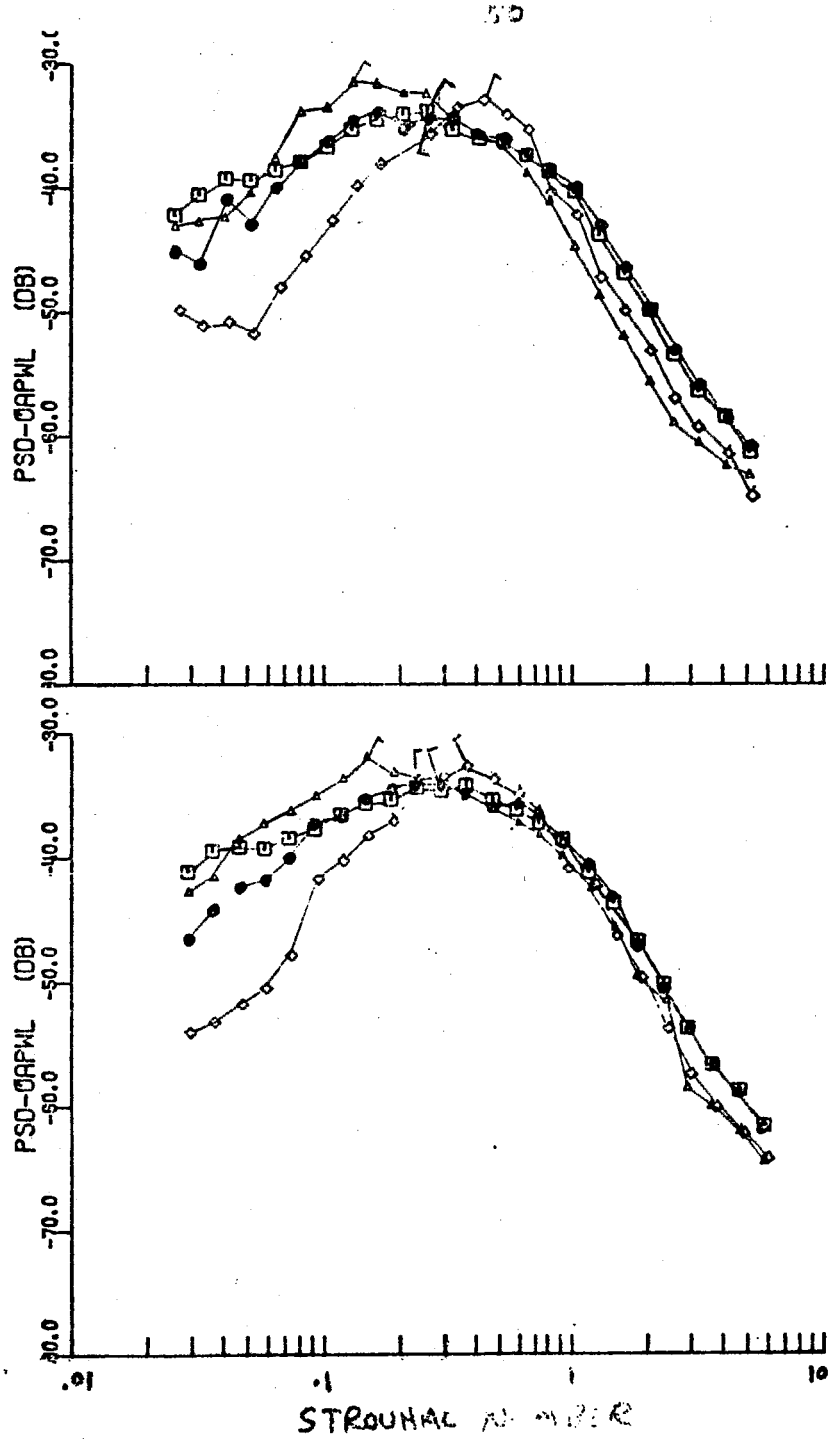

(c) P_c/P_o = .59

(d) P_c/P_o =.66

Figure 12. - Continued.

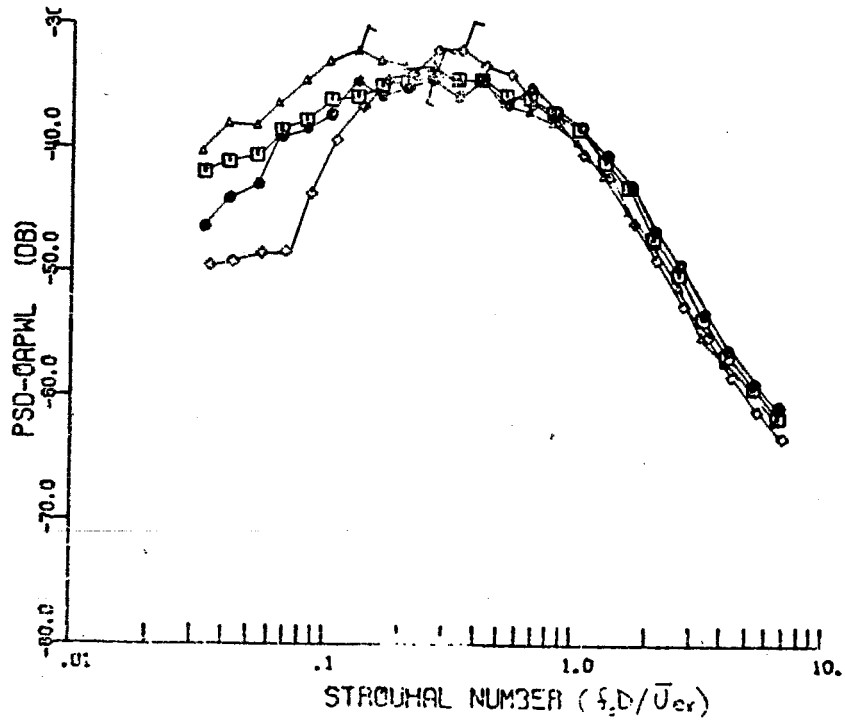

(e) P_c/P_o = .72

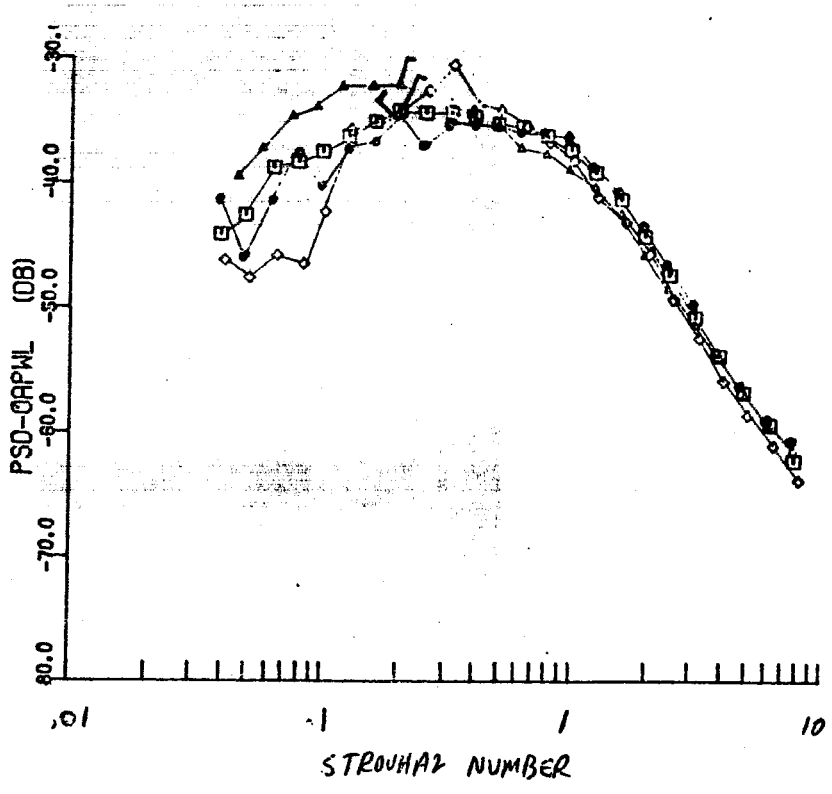

(f) P_c/P_o = .79

Figure 12. - Continued.

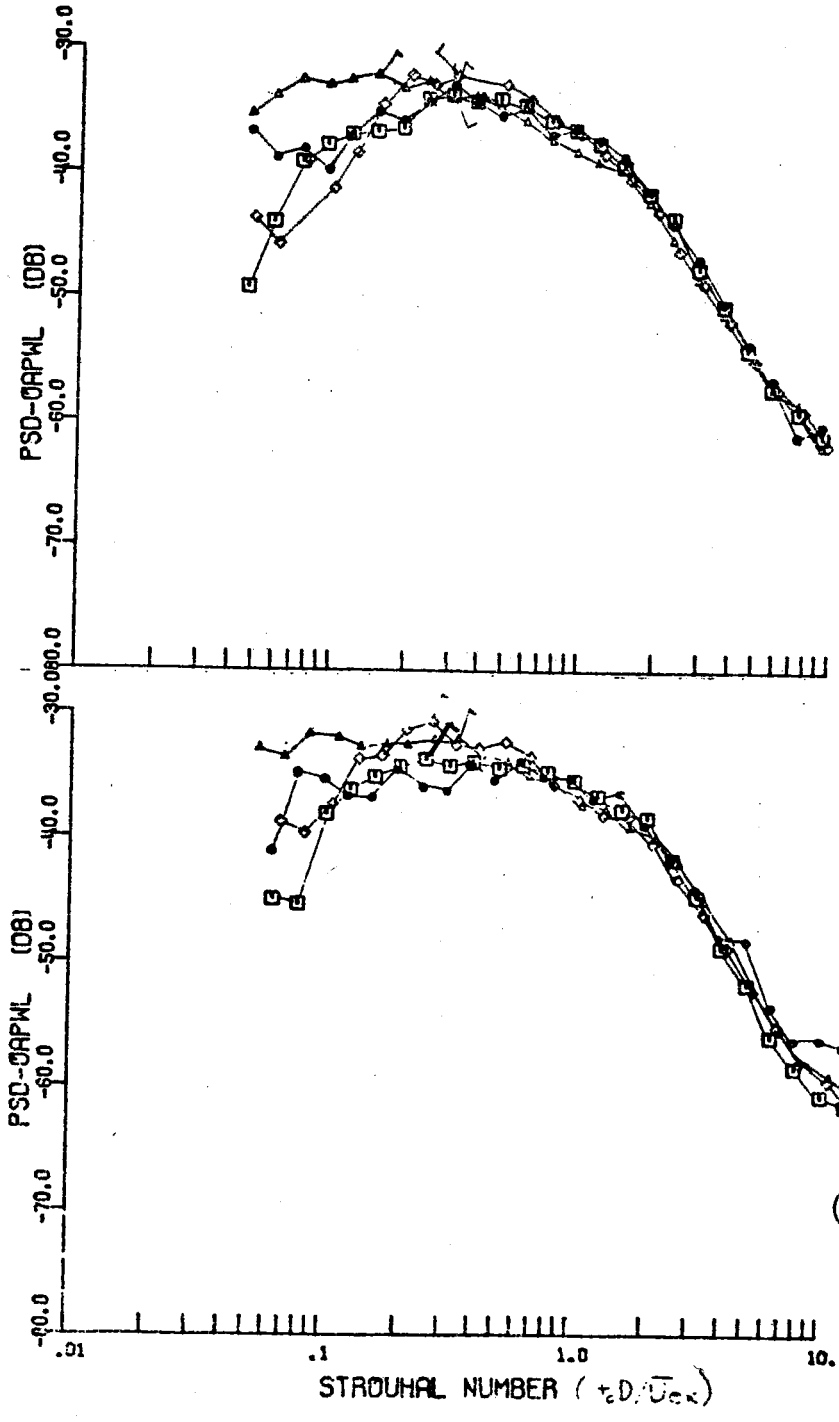

(g) $P_c/P_o = .86$

(h) $P_c/P_o = .92$

Figure 12. - Concluded.

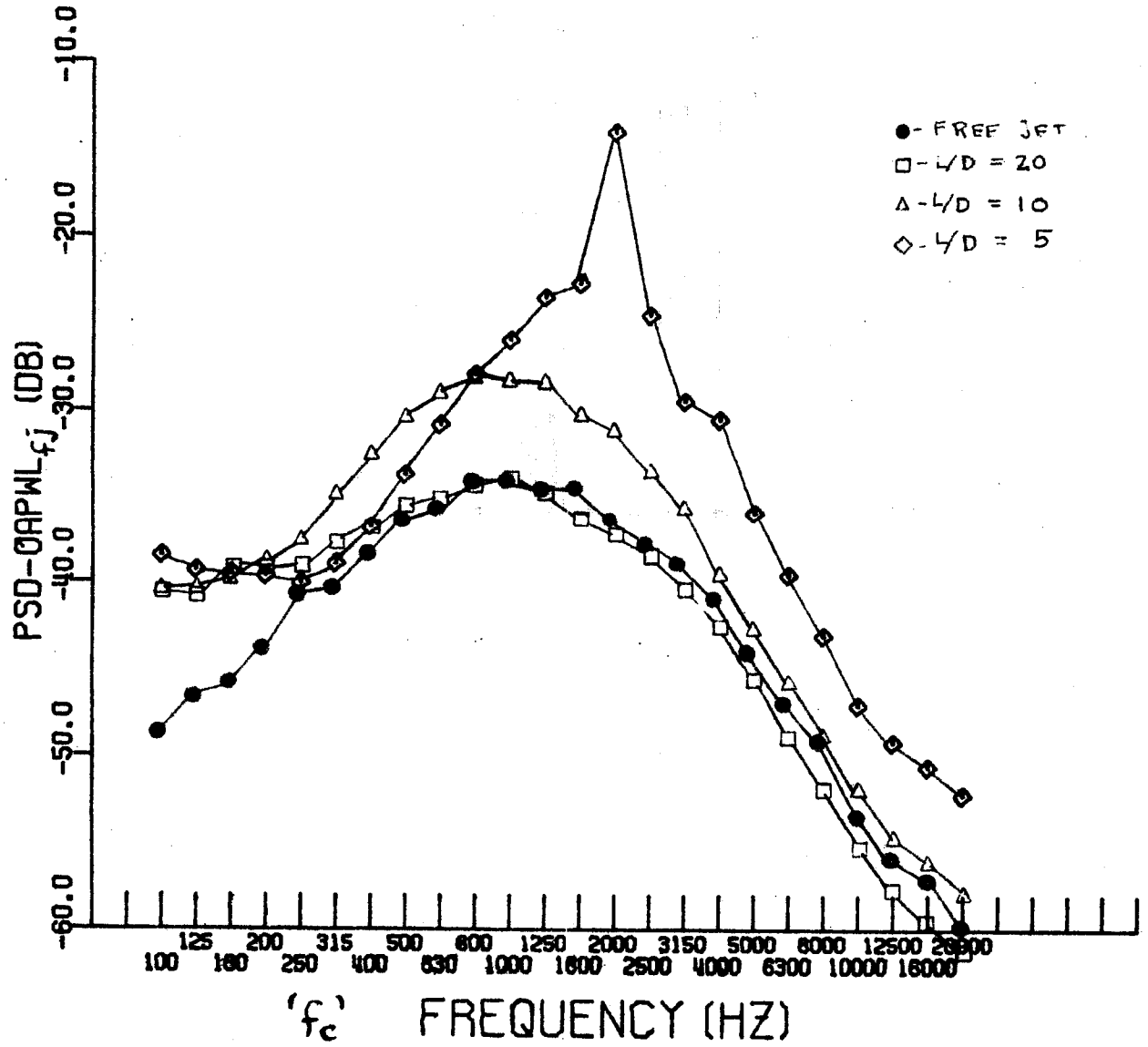

(a) U_{ex} = 293 m/s (P_c/P_o = .47)

Figure 13. - Power spectra normalized to free-jet overall power levels.

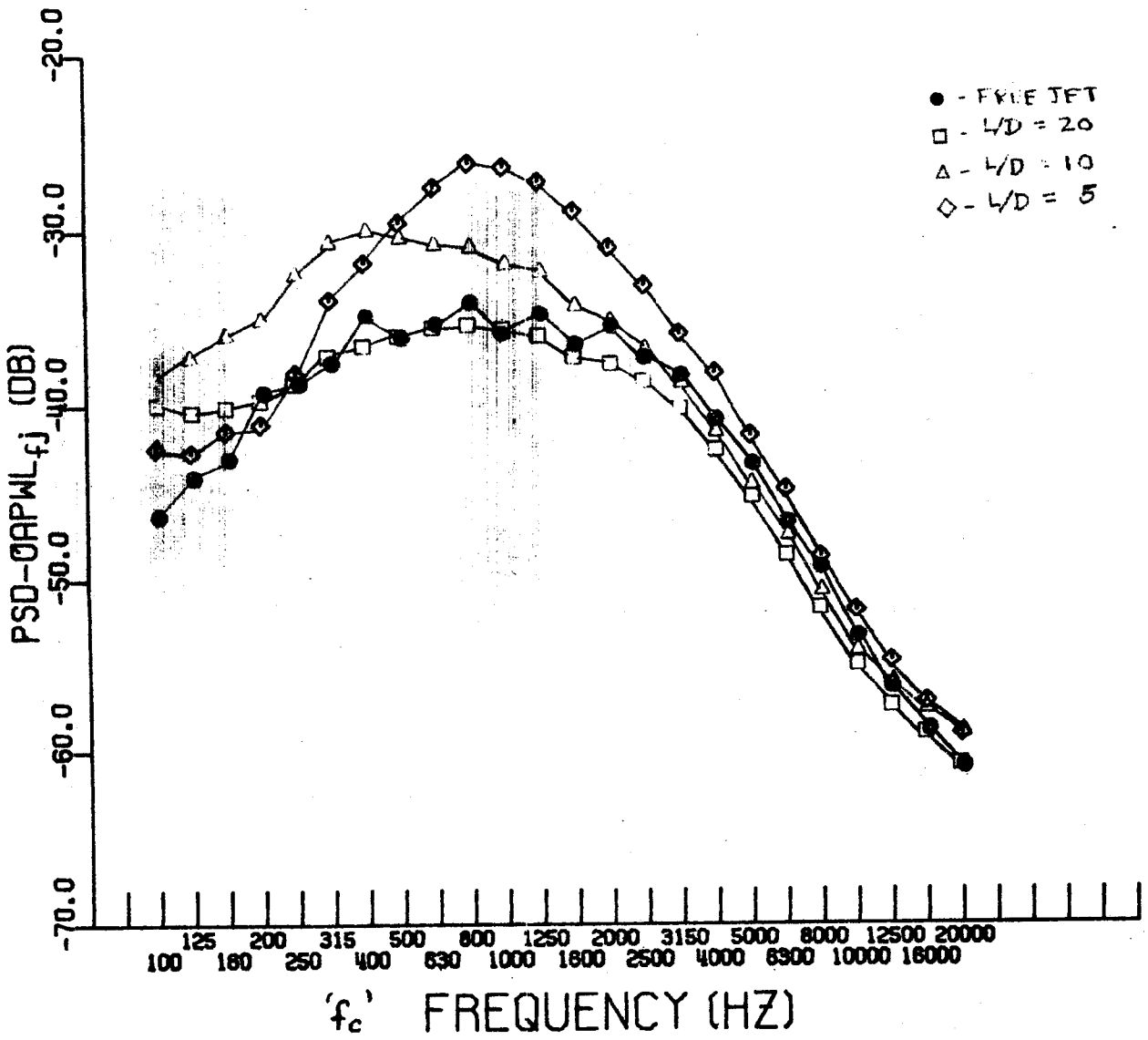

(b) U_{ex} = 186 m/s (P_c/P_o = .72)

Figure 13. - Continued.

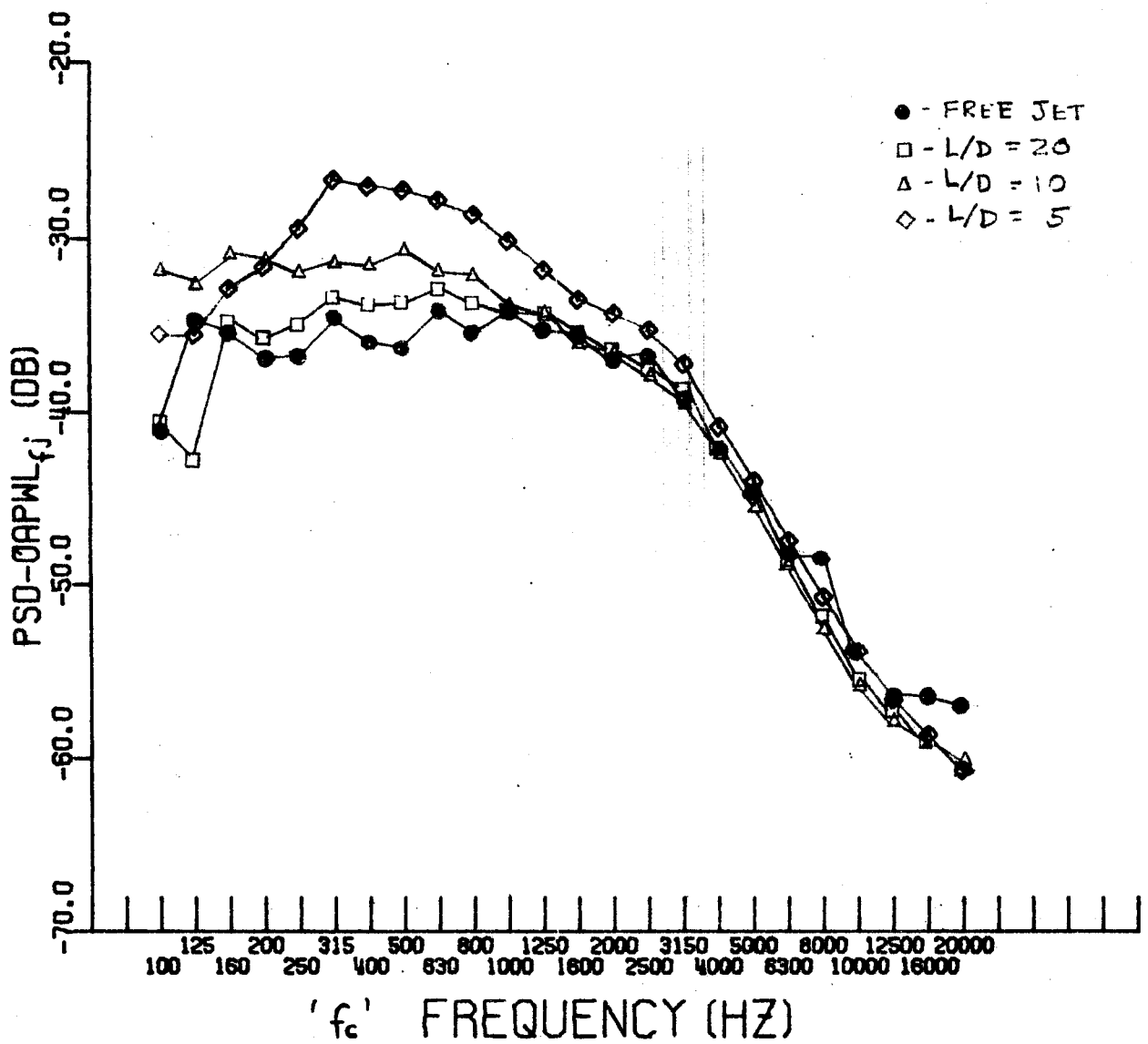

(c) U_{ex} = 98 m/s (P_c/P_o = .92)

Figure 13. - Concluded.

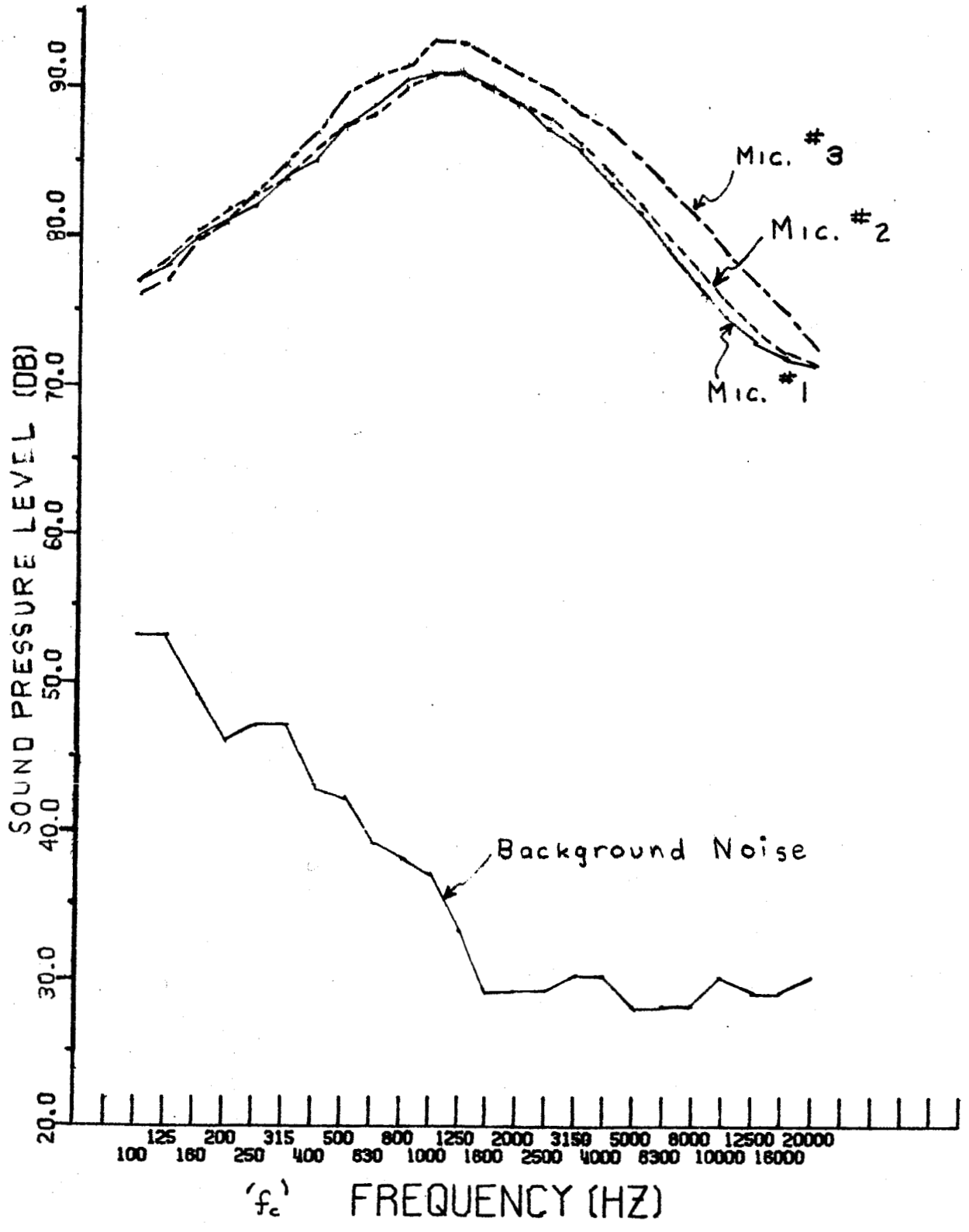

Figure 14. - Sample reverberant room microphone measurements and background noise. L/D = 20. U_{ex} = 290 m/s

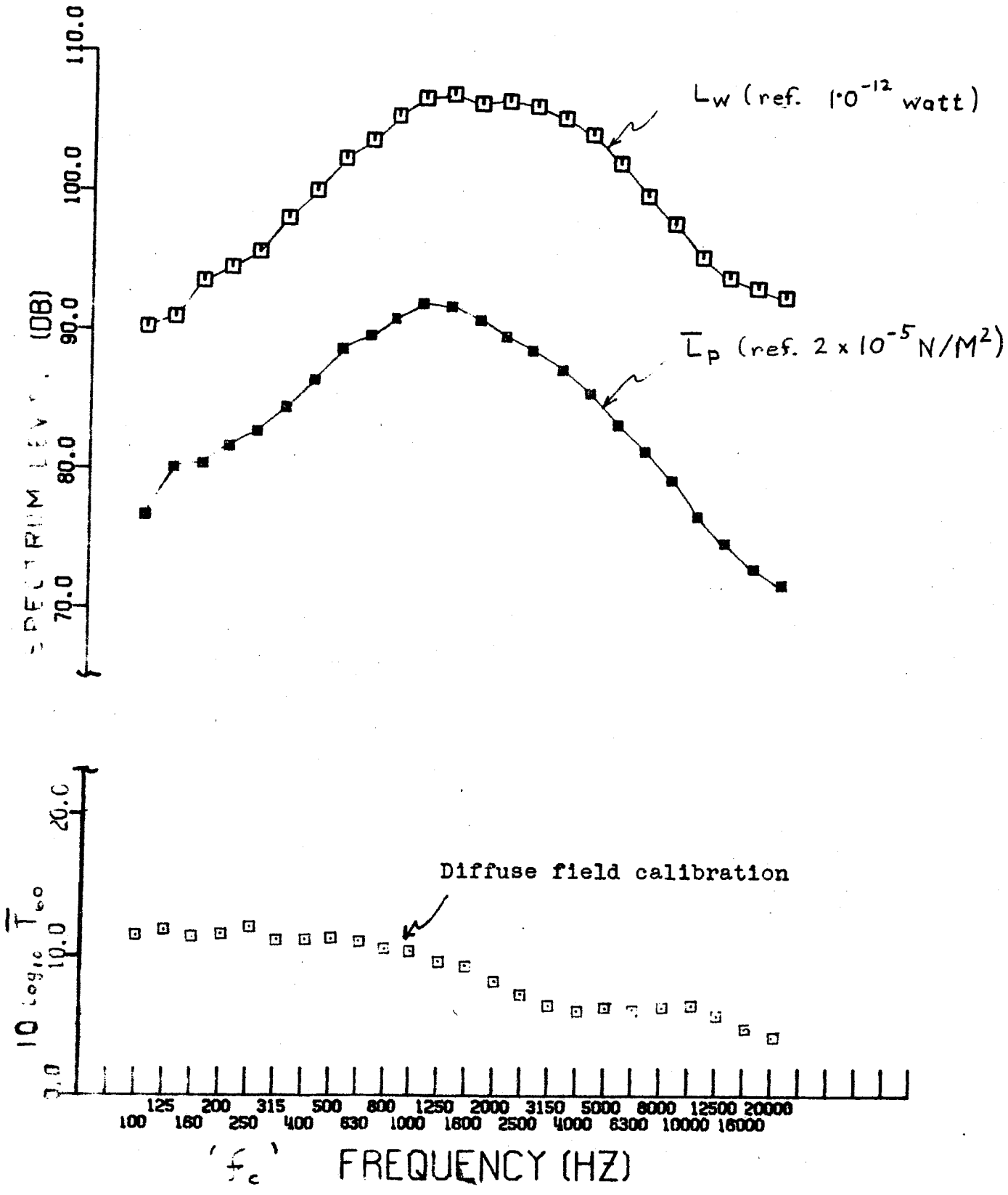

Figure 15. - Sample diffuse field calibration correction, sound pressure level, and power spectra. L/D = 20. U_{ex} = 290 m/s.